Raymo, M.E., Jansen, E., Blum, P., and Herbert, T.D. (Eds.), 1999
Proceedings of the Ocean Drilling Program, Scientific Results, Vol. 162

9. MAGNETIC STRATIGRAPHY AT SITES 907 AND 985 IN THE NORWEGIAN-GREENLAND SEA AND A REVISION OF THE SITE 907 COMPOSITE SECTION[1]

J.E.T. Channell,[2] Alejandro E. Amigo,[2] T. Fronval,[3] F. Rack,[4] and B. Lehman[5]

ABSTRACT

The magnetic polarity stratigraphy at Site 907 obtained from the shipboard pass-through magnetometer and from discrete samples is readily interpretable back to the onset of the Gilbert Chron (5.89 Ma). From this level to the base of the section at ~14 Ma, the interpretation is corroborated by silicoflagellate datums with predictable correlation to polarity chrons. The resulting magnetostratigraphic interpretation differs from those proposed in the Leg 151 (Hole 907A) and 162 (Holes 907B and 907C) *Initial Reports* volumes. An important hiatus in the 7–10 Ma interval at Site 907 caused sedimentation to slow or cease for ~2.7 m.y. We have revised the shipboard correlation among the three holes at Site 907, resulting in a new composite section splice and recalculation of composite depths.

For Site 985, magnetostratigraphic interpretation is possible down to ~150 meters below seafloor (mbsf) (C3An/C3Ar) at ~6 Ma. There are no useful biostratigraphic datums from Site 985 to support this interpretation; however, the interpretation is supported by the correlation of Sites 985 and 907 using natural gamma data from the shipboard multisensor track. Below ~150 mbsf at Site 985, drilling-related deformation at the onset of extended core barrel drilling precluded magnetostratigraphic interpretation.

INTRODUCTION

Sites 907 and 985 are located on the Iceland Plateau (Fig. 1) and are part of a paleoenvironmental transect from the Vøring Plateau (Sites 642–644, Leg 104) to the Greenland margin (Site 987). The objectives at these sites are to monitor the climatically sensitive and variable thermal gradients between the polar areas near Greenland and temperate areas off Norway, derive an open-ocean record of ice-rafted debris (IRD) and carbonate accumulation, and document the history of the formation of northern-source deep waters. Piston cores from the southern Nordic seas have shown that warm climatic intervals were short and poorly developed during the late Quaternary (Heinrich and Baumann, 1994; Fronval and Jansen, 1996). A major objective at Sites 907 and 985 was to extend the record back in time and gauge the longer term evolution, particularly of interglacial intervals.

Hole 907A was drilled in August 1993 during Ocean Drilling Program (ODP) Leg 151. Plans for further holes at this site were abandoned because of a medical evacuation. Site 907 was reoccupied during Leg 162 when two additional holes (Holes 907B and 907C) were drilled.

Site 985 is located in a deeper part of the Norway Basin, at 2788 m water depth, a depth ~1000 m deeper than that at Site 907 (Fig. 1). In addition to the objectives mentioned above, Site 985, located on Eocene Anomaly 22, was chosen to recover both Neogene and Paleogene sections to monitor the long-term paleoceanographic evolution.

MAGNETIC STRATIGRAPHY

Methods

Archive halves of core sections were measured using the shipboard cryogenic pass-through magnetometer. A few cores from the base of the advanced piston cored (APC) section at Site 907 were not measured because of excessive drilling-related deformation, and, at Hole 985A, measurements were discontinued below 180 meters below seafloor (mbsf) because of excessive drilling-related deformation in the extended core barrel section. Stepwise alternating field (AF) demagnetization was not feasible during the cruise, and most core sections were measured on board ship at a single demagnetization step (generally 25 mT). The choice of peak AF field was based on stepwise demagnetization of a few core sections and a handful of discrete samples.

The shipboard pass-through magnetometer data are perturbed by (1) magnetic overprints derived from the drill string, (2) drilling- and dropstone-related core deformation, and (3) diagenetic (secondary) remanence acquisition associated with formation of iron sulfides, particularly in ash-rich layers. Drilling-related deformation and dropstones can be avoided by discrete sampling. In addition, a complete demagnetization sequence can be performed on discrete samples to "ground truth" the shipboard magnetic stratigraphy.

Discrete samples were collected during the cruise in the standard 7-cm^3 plastic boxes and measured at laboratories at Gif-sur-Yvette and at the University of Florida. Natural remanent magnetization was measured before demagnetization and during stepwise AF demagnetization using a peak field increment of 5 mT in the 5–70 mT range, or until the magnetization intensity fell below magnetometer noise level. Orthogonal projections of AF demagnetization data indicated that a characteristic magnetization component could usually be resolved at peak alternating fields above ~20 mT. A lower coercivity component was observed in most samples, particularly those with a reverse polarity characteristic component. The low-coercivity component is oriented steeply downward and is probably a viscous remanent magnetization imposed by the drill-string assembly. The characteristic (higher coercivity) magnetization component was picked visually from orthogonal projections of demagnetization data, and its

[1]Raymo, M.E., Jansen, E., Blum, P., and Herbert, T.D. (Eds.), 1999. *Proc. ODP, Sci. Results*, 162: College Station, TX (Ocean Drilling Program).

[2]Department of Geology, University of Florida, Gainesville, FL 32611-2120, U.S.A. Channell: jetc@nersp.nerdc.ufl.edu

[3]Department of Geology, University of Copenhagen, DK-1350 Copenhagen, Denmark.

[4]Department of Geodesy and Geomatics Engineering, University of New Brunswick, Fredericton, NB E3B 5A3, Canada.

[5]Laboratoire des Sciences du Climat et de l'Environnement, CNRS-CEA, Avenue de la Terrasse, 91198 Gif-sur-Yvette, France.

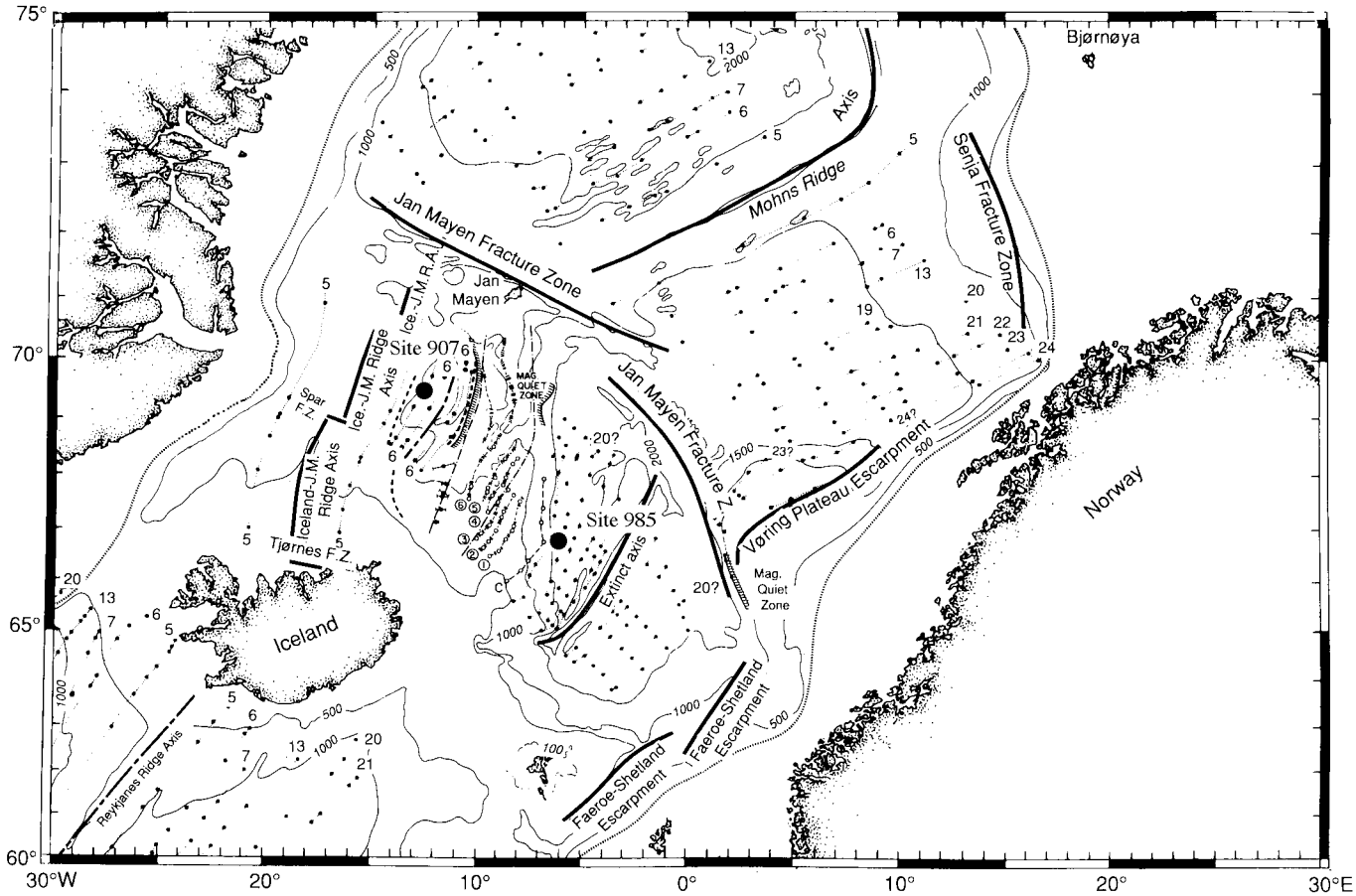

Figure 1. Location map for Sites 907 and 985 indicating oceanic magnetic anomaly numbers (after Talwani and Eldholm, 1977). J.M. = Jan Mayen, F.Z. = Fracture Zone, Mag. = Magnetic.

direction was computed using the standard least-squares technique (Kirschvink, 1980).

Site 907

Orthogonal projections of incremental AF demagnetization of discrete samples indicate that a characteristic magnetization component can be resolved at peak fields above ~20 mT (Fig. 2). The drill string–related magnetic overprint is apparent as a steep downward low-coercivity component in most samples, particularly those in which the characteristic component has reverse polarity.

For the upper 110 m at Site 907, the shipboard pass-through inclination data (after AF demagnetization at peak fields of 25 mT) indicate clearly defined polarity zones (Fig. 3), although the records are perturbed by core deformation, abundant ash layers, and associated secondary magnetizations produced by authigenic iron sulfides. Core deformation at Site 907 is exacerbated by abundant dropstones. The component inclinations determined from discrete samples at Hole 907B generally ratify the polarity stratigraphy from shipboard data (Fig. 3); however, comparison of the shipboard data (including Hole 907A from Leg 151) indicate significant discrepancies among the three holes in the placement of some polarity zone boundaries. These discrepancies are not accounted for when depths in mbsf are converted to meters composite depth (mcd) using the shipboard calculations. In addition, high-resolution IRD counts indicated that some glacial periods were missing and that others were repeated when using the shipboard composite section. By creating a new composite depth scale, we removed several instances of "double-coring" (overlap between cores), which resulted from the shipboard calculations.

The shipboard composite depth scale for Site 907 was revised by aligning the complementary gamma-ray attenuation porosity evaluator (GRAPE) and magnetic susceptibility data from each hole, with emphasis given to the matches between Holes 907A and 907C. Data from Hole 907B were used to resolve uncertainties in the correlations between Holes 907A and 907C. The methods used were similar to those used to construct composite depth sections during Leg 138 (Hagelberg et al., 1992) and during subsequent ODP legs, including Leg 162 (see Jansen, Raymo, Blum, et al., 1996). Drilling-related deformation was apparent in some parts of the GRAPE and magnetic susceptibility records and confirmed by comparison with the shipboard core descriptions. No differential stretching or squeezing was introduced within individual cores. After construction of the composite depth section, a spliced record representative of the multiply cored sedimentary sequence was assembled.

Most ash layers in the upper 100 mbsf of Hole 907A are associated with reduced GRAPE bulk density and increased magnetic susceptibility values relative to the mean values for these sediments (Rack et al., 1996). In the deeper parts of Hole 907A, below ~100 mbsf, the situation is different (ashes have higher bulk density and higher magnetic susceptibility relative to mean values) because of the relative dominance of low-density biosiliceous microfossils whose presence largely controls the measured sediment physical and geotechnical properties. The bulk of the ash layers in Hole 907A have been "ground truthed" by discrete sampling and petrologic analyses reported by Lacasse et al. (1996) and Werner et al. (1996). These authors used the above-mentioned, distinctive "signature" of these tephra layers to rapidly locate thin ash layers and intervals of dispersed or disseminated ash. The peaks in magnetic susceptibility associated

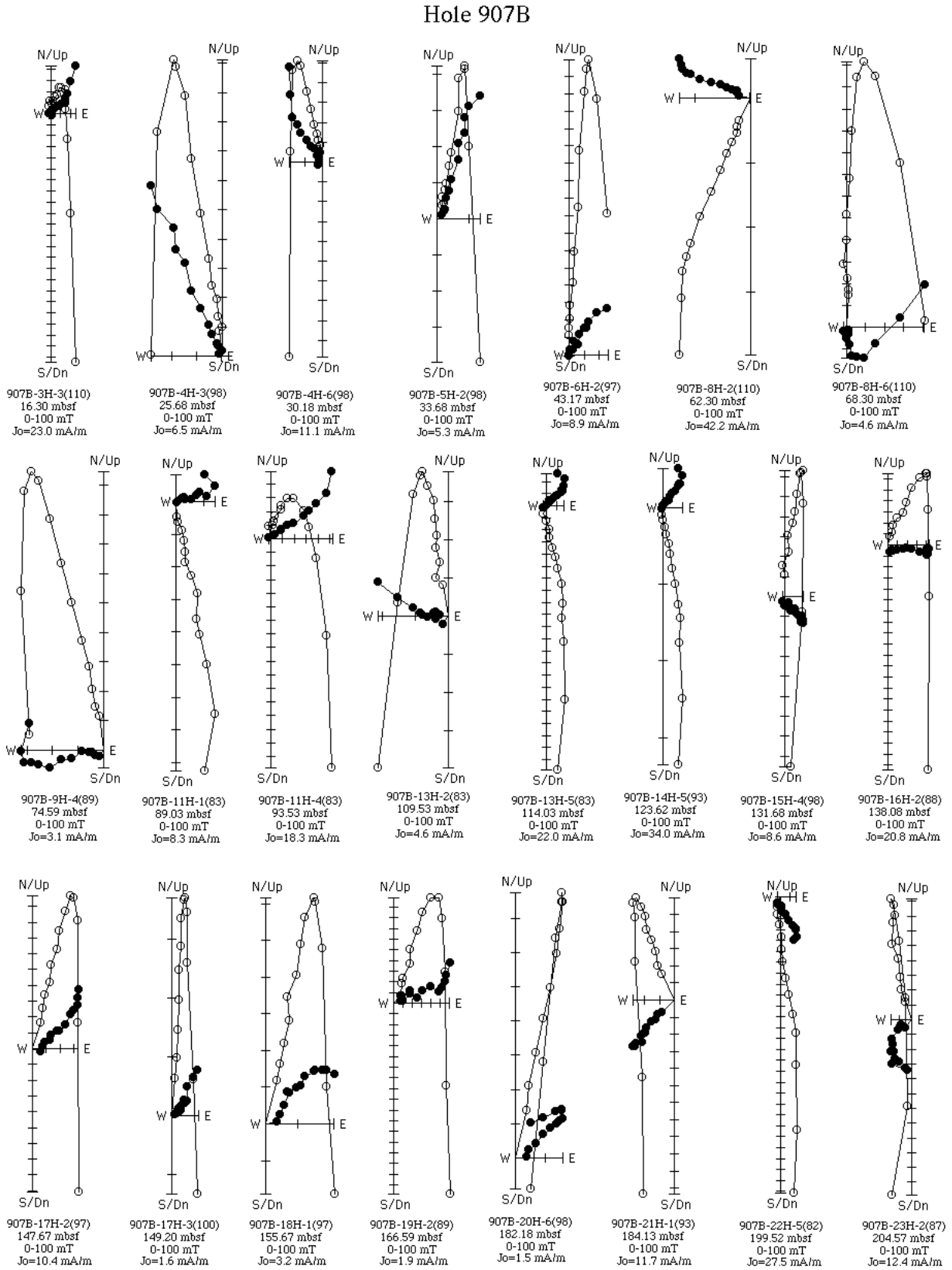

Figure 2. Orthogonal projection of AF demagnetization data from discrete samples in the 0–210 mbsf interval of Hole 907B. Open and solid symbols indicate projections on the vertical and horizontal planes, respectively. J_0 = magnetization intensity before demagnetization, Dn = down. Numbers in parentheses indicate sample location (in centimeters).

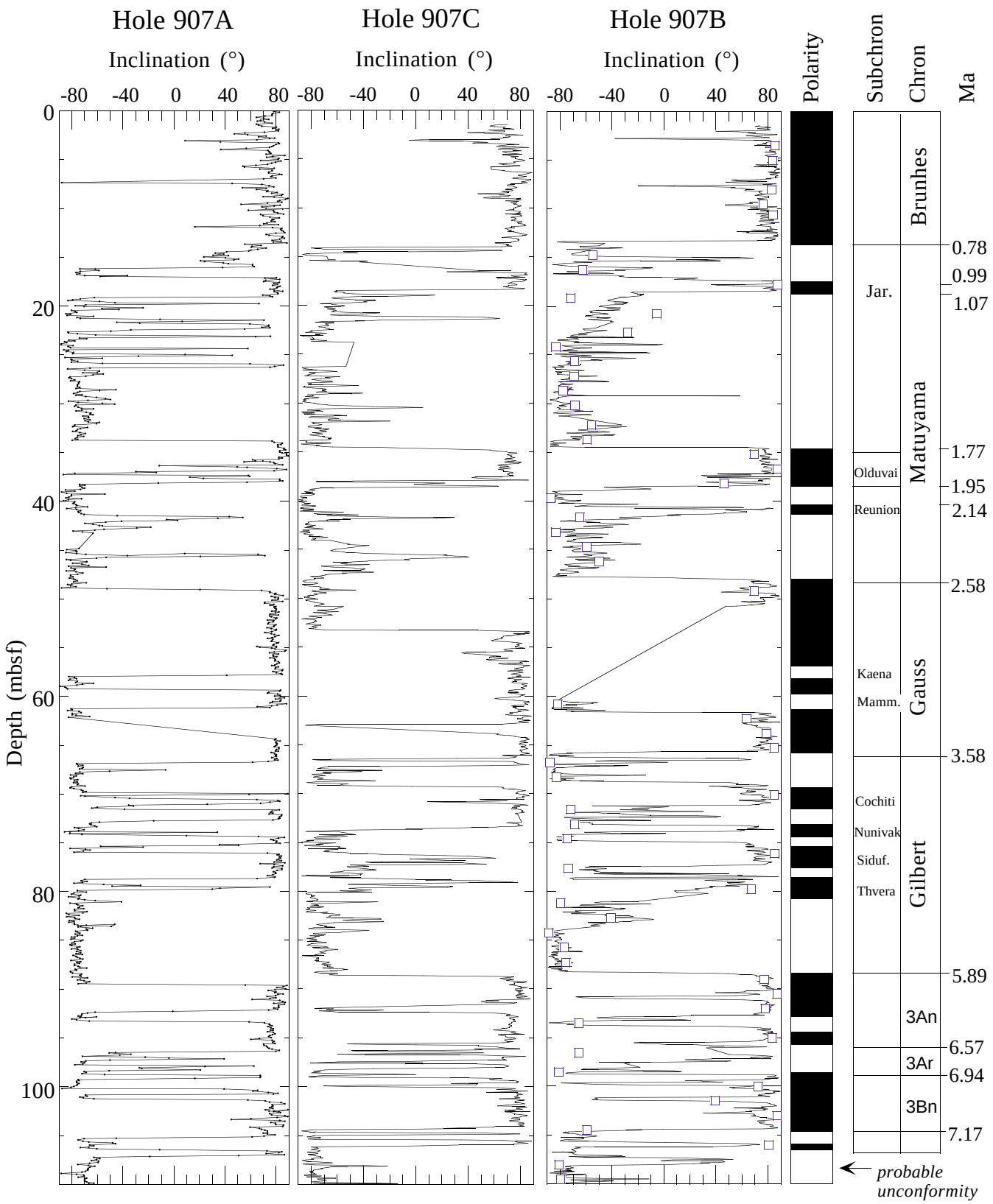

Figure 3. Shipboard (pass-through magnetometer) inclination data after AF demagnetization at peak fields of 30 mT for Hole 907A, and 25 mT for Holes 907B and 907C, in the 0–110 mbsf interval. Open squares indicate component inclinations determined from discrete (7 cm^3) samples measured postcruise. Component directions were computed from orthogonal projections of AF demagnetization data. Hole 907A data are from Leg 151 (Shipboard Scientific Party, 1995). Absolute ages of polarity chron boundaries from Cande and Kent (1995). Jar. = Jaramillo, Mamm. = Mammoth, Siduf. = Sidufjall.

with both discrete and dispersed ash layers are linked to an abundance of magnetite-bearing crystals, basaltic components (sideromelane and tachylite), or shards coated by iron sulfide. High volcanic glass concentrations were found in the sand and silt component of dispersed ash zones. The ash zones were difficult to locate visually, but they could be identified using the magnetic susceptibility record (Lacasse et al., 1996) and hence correlated from Hole 907A with similar intervals in Holes 907B and 907C (Fig. 4).

Recalculated composite depths for Site 907 and the splice for the composite section are given in Appendixes A and B, respectively. Examples of these correlations are given in Figure 4 and Table 1. In general, the new composite depth (mcd) calculations are consistent for polarity zone boundaries from the three holes. The apparent position of the Brunhes/Matuyama boundary in Hole 907A (Fig. 3; Table 2) remains inconsistent, however, and the base of the Olduvai/Reunion interval at Hole 907A is also anomalous (Figs. 3, 4B; Table 2).

The interpreted position of the Brunhes/Matuyama boundary in Hole 907A coincides with a 10-cm-thick ash layer, designated as Layer G by Lacasse et al. (1996). A large dropstone was recovered just above this ash layer, at interval 162-907A-2H-6, 124–129 cm (Shipboard Scientific Party, 1995). The large dropstone in this core very likely disrupted both the sedimentary structure and the magnetic measurements across this interval, possibly resulting in a downward shift of the apparent (interpreted) position of the Brunhes/Matuyama boundary in Hole 907A. The same ash layer appears, both without a large dropstone in Hole 907B (interval 162-907B-3H-2, 65–77 cm; 14.35–14.47 mbsf) and with a large overlying dropstone in Hole 907C (interval 162-907C-2H-6, 145 cm, through 2H-7, 6 cm; 15.05–15.16 mbsf). In both cases, the ash layer is located below the interpreted Brunhes/Matuyama boundary. Therefore, it seems likely that the true position of the Brunhes/Matuyama boundary in Hole 907A should be placed at ~15 mbsf, which would be consistent with the composite depths determined for this feature in the other two holes (Table 2).

The position of the base of the Olduvai Subchron in Hole 907A is likely located within the core break between Cores 162-907A-4H and 5H, where a significant gap in core recovery is suggested by the new composite depth scale (see Fig. 4A, B). The normal polarity interval at the top of Core 162-907A-5H would then be assigned to the Reunion Subchron. The base of this normal polarity interval is located about the same distance above an ash layer as the inferred position of the Reunion Subchron in Core 162-907B-6H, where the ash is located at 43.5 mbsf (Fig. 4B). The small normal polarity interval at 41.67–41.83 mbsf in Hole 907C (Core 162-907C-5H) should correlate in some way to the base of Core 162-907B-5H, which suggests that the bulk of the Reunion should be located within the lower part of Core 162-907C-5H.

The 50–60 mbsf interval at Hole 907B is a data gap (Fig. 3) resulting from the high degree of drilling-related deformation in Core 162-907B-7H. The top and base of the Gilbert Chron are consistent at the three holes, but the subchrons within the Gilbert Chron are not easily correlated among them. Similarly, below the Gilbert Chron, the polarity pattern is not easily correlated among the three holes. We attribute these inconsistencies to disruption of the polarity zone pattern by drilling-related remagnetization and core deformation.

For the 110–185 mbsf interval at Site 907, the correlation among the three holes is fairly straightforward (Fig. 5). Below 185 mbsf, the record is perturbed by core deformation at the base of the APC section.

Site 985

As at Site 907, orthogonal projections of incremental AF demagnetization for Site 985 indicate that a characteristic magnetization component can be defined, after removal of a steep downward (drill string–related) magnetic overprint (Fig. 6).

Shipboard pass-through magnetometer data (after demagnetization of peak fields of 25 mT) indicate a well-defined magnetic stratigraphy to the base of the Gauss Chron (95 mbsf) (Fig. 7). The records are perturbed by core deformation exacerbated by numerous dropstones and by ash layers with localized iron sulfide diagenesis. Authigenic iron sulfide formation affects the primary magnetization because of associated detrital magnetite dissolution and the presence of secondary chemical remanences associated with some iron sulfide compositions. Deformation in Cores 162-985A-3H and 162-985B-3H resulted in poor definition of the Brunhes/Matuyama boundary at both holes. Remagnetization results in poor definition of the Gilbert Chron. Below the Gilbert Chron, the record may be affected by increased core deformation at the base of the APC section. Component inclinations determined from discrete samples from Hole 985A ratify the shipboard magnetic stratigraphy as far down as the base of the Gauss Chron (Fig. 7). The component inclinations of discrete samples do not clearly define the normal polarity intervals within the Gilbert Chron, although the boundaries of the Gilbert can be located. Below the Gilbert Chron, discrete sample inclinations appear to define several polarity zones although, in this part of the section, the characteristic magnetization component is less well defined because of incomplete removal of secondary magnetization components.

POLARITY CHRON INTERPRETATIONS

Site 907

Two alternative interpretations of the Site 907 magnetic stratigraphies were presented in the Leg 162 *Initial Reports* volume (Shipboard Scientific Party, 1996a). One of these interpretations (Interpretation 1 in Fig. 8) implies hiatuses in deposition at ~105 mbsf and at ~140 mbsf. The other interpretation (Interpretation 2 in Fig. 8) implies a more uniform sedimentation rate without major hiatuses. Interpretation 1 is essentially the same as the interpretation given for Hole 907A in the Leg 151 *Initial Reports* volume (Shipboard Scientific Party, 1995).

Shipboard biostratigraphy had insufficient resolution to distinguish between the two alternative magnetostratigraphic interpretations. Except in the top few cores, calcareous microfossils are absent. Silicoflagellates and diatoms are preserved at Site 907, particularly in the 50–100 mbsf interval, but shipboard study was too cursory to provide useful biostratigraphic constraints. Since the Leg 162 cruise, detailed shore-based studies on diatoms from Hole 907A have led to a correlation of middle Miocene to late Pliocene diatom events with the polarity time scale (Koç and Scherer, 1996). These authors modified the original magnetostratigraphic interpretation at Hole 907A in making these biomagnetostratigraphic correlations.

Neogene diatoms evolved rapidly in the high-latitude oceans, and therefore have high potential for biostratigraphy. However, diatoms of the Norwegian-Greenland Sea are endemic, and correlations established in the North Atlantic or North Pacific are not necessarily applicable to the Norwegian-Greenland Sea. No diatom zonation was established from Leg 104 (Vøring Plateau) sediments. The few diatom events documented on the Vøring Plateau cannot be unambiguously correlated with polarity chrons because of uncertainties in pre-Pleistocene magnetostratigraphic interpretations. At Hole 907A, Norwegian-Greenland Sea diatom biostratigraphy has taken a giant leap forward with the establishment by Koç and Scherer (1996) of eleven diatom "intervals" (zones) from middle Miocene to Holocene. Hole 907A now provides a reference section for diatom stratigraphy from the Norwegian-Greenland Sea, and it is important to establish the correlation of this zonal scheme with the polarity time scale. The correlation of the diatom "intervals" with the polarity time scale advocated by Koç and Scherer (1996) is based on a reinterpretation of the Hole 907A (Leg 151) magnetostratigraphy (Shipboard Scientific Party, 1995).

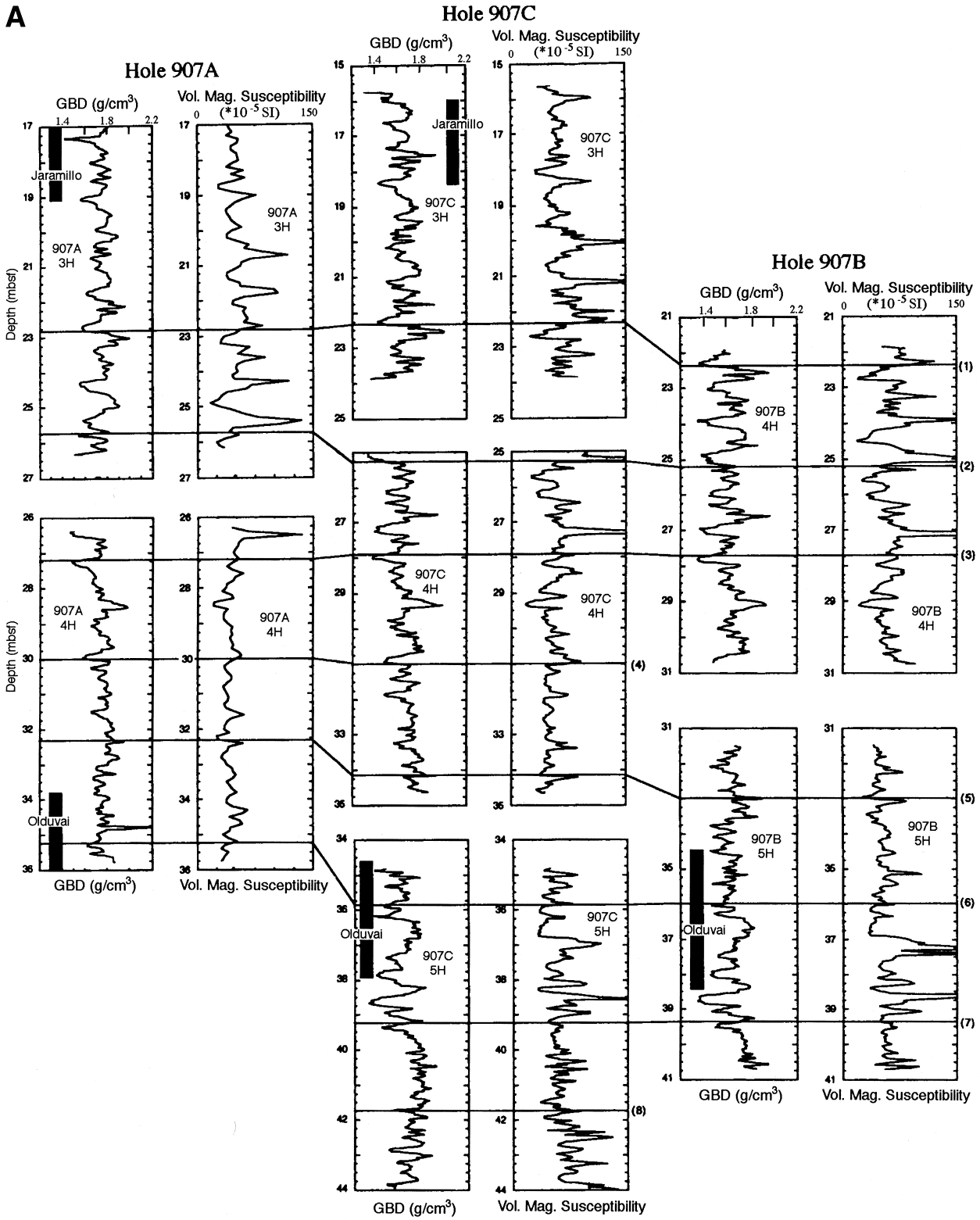

Figure 4. **A.** GRAPE bulk density (GBD) and volume (vol.) magnetic susceptibility for the Cores 3H–5H interval for Holes 907A, 907B, and 907C. Tie lines among the holes (Table 1) were used to calculate composite depths (Appendix A) and to construct a splice for the composite section (Appendix B). (Continued on next page.)

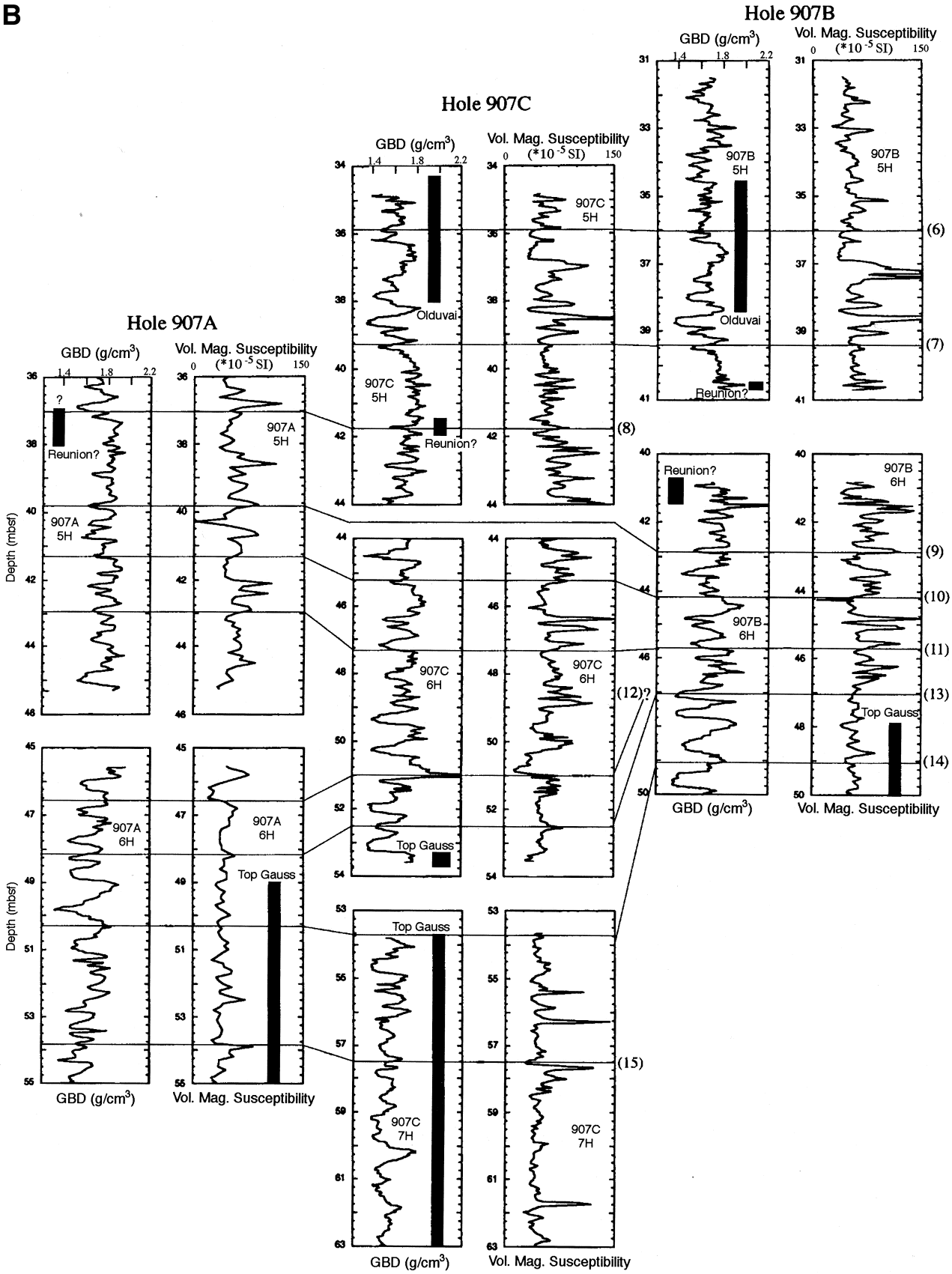

Figure 4 (continued). **B.** GRAPE bulk density (GBD) and volume (vol.) magnetic susceptibility for the Cores 5H–7H interval for Holes 907A, 907B, and 907C. Tie lines among the holes (Table 1) were used to calculate composite depths (Appendix A) and to construct a splice for the composite section (Appendix B). (Continued on next page.)

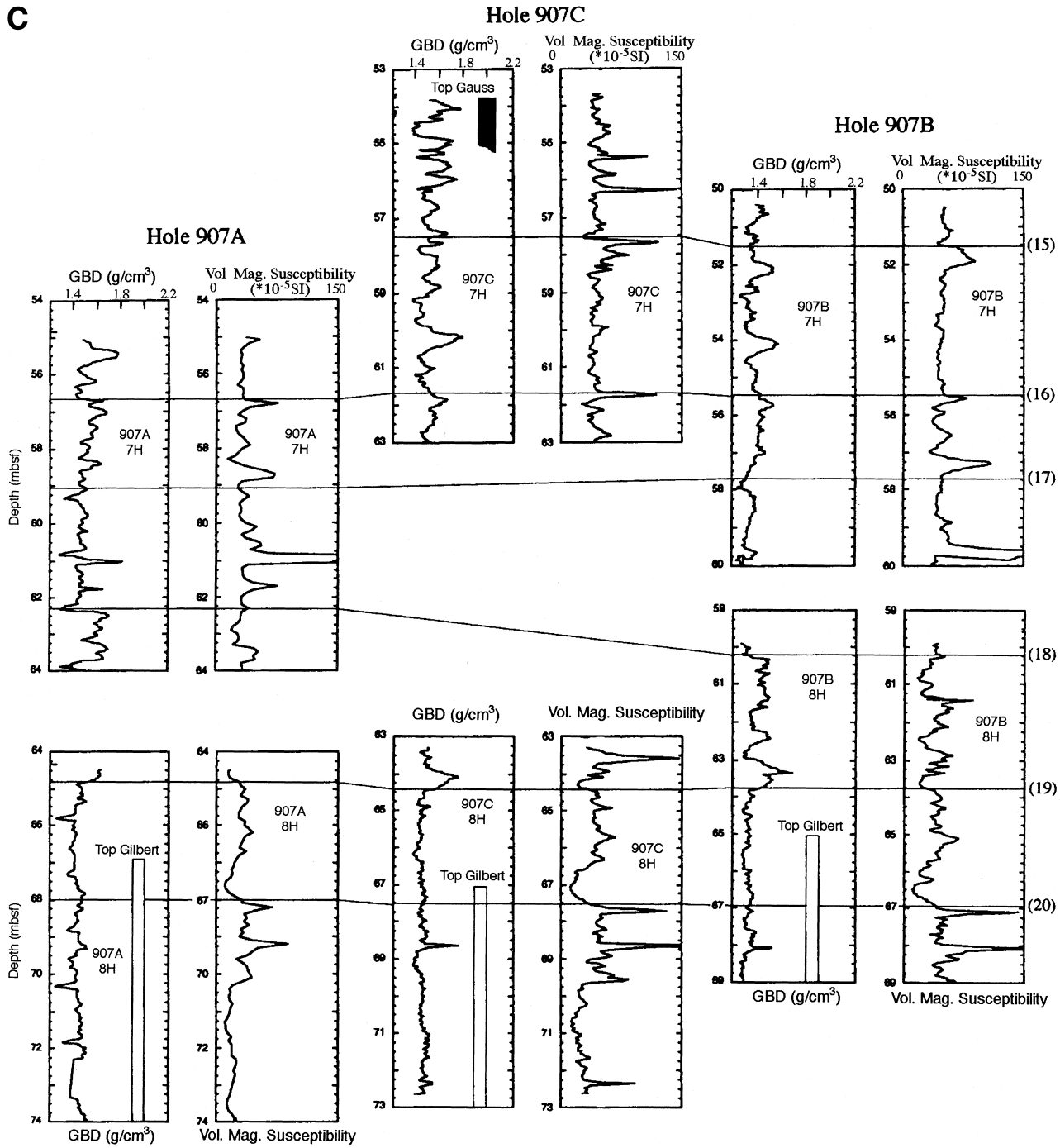

Figure 4 (continued). **C.** GRAPE bulk density (GBD) and volume (vol.) magnetic susceptibility for the Cores 7H–8H interval for Holes 907A, 907B, and 907C. Tie lines among the holes (Table 1) were used to calculate composite depths (Appendix A) and to construct a splice for the composite section (Appendix B).

The endemic nature of Norwegian-Greenland Sea diatoms, the lack of existing correlations of diatoms with the polarity time scale in this region, and uncertainty in the interpretation of the Site 907 magnetostratigraphy (see Fig. 8) means that there are few constraints on possible biomagnetostratigraphic correlations. Silicoflagellates are well preserved throughout the middle Miocene–Pliocene interval at Site 907 (see Amigo, Chap. 5, this volume), and they provide a means of constraining the magnetostratigraphic interpretations. Silicoflagellates are generally less endemic than diatoms, and silicoflagellate datums recognized at Site 907 can be used to "pin" the magnetostratigraphic interpretation. Site 982, drilled during Leg 162 on the Rockall Plateau, has proved useful in this respect. This site has well-preserved silicoflagellate and calcareous nannofossil records (Amigo, Chap. 5, this volume; Shipboard Scientific Party, 1996b), allowing a correlation of critical silicoflagellate datums with nannofossil zones and hence with the polarity time scale.

In Hole 907B, the last occurrence (LO) datums of silicoflagellates *Bachmannocena apiculata apiculata* and *Bachmannocena apiculata curvata* appear together at 190.26 mbsf with the first occurrence (FO) of *Bachmannocena circulus apiculata* found just below, at 193.79 mbsf. In Hole 982B, the same occurrence overlap is present in the 444–454 mbsf interval, and the short-ranging species *Distephanus*

stauracanthus occurs within the overlap interval at 449 mbsf. This unique and stratigraphically significant juxtaposition of silicoflagellate datums has been recognized at many locations; the closest geographically (to Site 907) are Deep Sea Drilling Project (DSDP) Site 408 in the North Atlantic (Bukry, 1979) and ODP Site 642 on the Vøring Plateau (Locker and Martini, 1989). For Site 408 and Hole 982B (Bukry, 1979; Shipboard Scientific Party, 1996a), the overlap of the silicoflagellate datums can be correlated with the lower part of nannofossil Zone CN5, close to the CN4/CN5 nannofossil zonal boundary (nannofossil zonation of Okada and Bukry, 1980). According to Berggren et al. (1995), the CN4/CN5 nannofossil zonal boundary lies close to the C5ABr/C5ACn polarity chron boundary.

Table 1. Correlation tie lines for Figure 4A–C.

	Hole 907A		Hole 907C		Hole 907B	
Tie lines*	Depth (mbsf)	Core	Depth (mbsf)	Core	Depth (mbsf)	Core
1	22.80	3H	22.30	3H	22.40	4H
2	25.75	3H	25.30	3H	25.25	4H
3	27.25	4H	28.00	4H	27.75	4H
4	30.00	4H	31.00	4H	30.80	4H
5	32.30	4H	34.20	4H	33.00	5H
6	35.25	4H	35.80	5H	36.00	5H
7	Gap		39.25	5H	39.45	5H
8	37.00	5H	43.75	5H	Gap	
9	39.80	5H	Gap		43.80	6H
10	41.30	5H	45.30	6H	44.25	6H
11	42.90	5H	47.30	6H	45.80	6H
12	46.60	6H	51.00	6H	Condensed	
13	48.15	6H	52.50	6H	47.00	6H
14	50.30	6H	54.00	7H	49.10	6H
15	53.75	6H	57.50	7H	51.50	7H
16	56.70	7H	61.70	7H	55.50	7H
17	59.00	7H	Gap		57.75	7H
18	62.30	7H	Gap		60.25	8H
19	64.80	8H	64.40	8H	63.75	8H
20	68.00	8H	67.50	8H	66.90	8H

Note: *See Figure 4A–C.

In Hole 982B, the CN5/CN6 nannofossil boundary (= middle/late Miocene boundary) occurs at 377 mbsf, based on the LO of the nannofossil *Coccolithus miopelagicus* (Shipboard Scientific Party, 1996b). According to Berggren et al. (1995), this nannofossil zonal boundary correlates with C5r.2r. The FO of the silicoflagellate *Bachmannocena diodon nodosa* at 408 mbsf in Hole 982B is, therefore, older than C5r.2r. In Hole 907B, the FO of *Bachmannocena diodon nodosa* occurs at 152.40 mbsf within a reversed polarity zone (Fig. 5), which must be older than C5r.2r.

With these constraints provided by the silicoflagellate datums, we propose a correlation of polarity zones at Site 907 with polarity chrons (Figs. 3, 7) that differs from those offered in the *Initial Report*s volumes (Shipboard Scientific Party, 1995, 1996a). The new interpretation (Interpretation 3 in Fig. 8) is almost identical to the reinterpretation of the Hole 907A magnetic stratigraphy offered by Koç and Scherer (1996). As mentioned above, the endemic nature of diatoms from the Norwegian-Greenland Sea indicates that diatom-magnetostratigraphic correlations from outside the region may not provide useful constraints. However, one species common to the Norwegian-Greenland Sea and the North Pacific, the short-ranging diatom *Denticulopsis praedimorpha*, is found in the 160–163 mbsf interval in Hole 907A, correlating with C5AAn, and in the same polarity chron at Site 884 (North Pacific) (Barron and Gladenkov, 1995).

The magnetostratigraphic interpretation indicates a hiatus (disconformity) in the 100–115 mbsf interval (Figs. 3, 8) in which deposition slowed dramatically or stopped for ~2.5 m.y. There are two additional lines of evidence for this hiatus. First, a series of sawtooth-like "steps" in GRAPE density between 112 and 103 mbsf, which overprint a decreasing trend in density from 118 to 100 mbsf (Fig. 9), are associated with a change in character of the magnetic susceptibility record, which shows anomalously low values over the same depth interval. These profiles may be interpreted to suggest either (1) rapid variations in lithology and induration within this interval (which may be related to changes in sediment accumulation rates) or (2) reversals in downhole geotechnical gradients caused by erosion and/or nondeposition of sediment. Second, Koç and Scherer (1996) noted that

Table 2. Polarity chron boundaries at Site 907.

		Hole 907A (Leg 151)		Hole 907B		Hole 907C	
Polarity chron boundary	Age	Depth (mbsf)	Depth (mcd)	Depth (mbsf)	Depth (mcd)	Depth (mbsf)	Depth (mcd)
Brunhes/Mat.	0.780	16.10	16.13*	13.32	14.89	14.03	14.89
Top Jaramillo	0.990	17.00	18.50	17.05	18.62	16.00	18.19
Base Jaramillo	1.070	19.10	20.60	18.53	20.10	18.43	20.62
Top Cobb	1.200					21.13	23.32
Base Cobb	1.200					21.45	23.64
Top Olduvai	1.770	33.80	36.53	34.48	36.46	34.68	36.77
Base Olduvai	1.950			38.47	40.45	37.93	40.02
Top Reunion	2.130			40.57	42.55	41.67	43.76
Base Reunion	2.140			41.50	44.75	41.83	43.92
Mat./Gauss	2.580	49.00	54.79	47.85	54.79	53.27	54.88
Top Kaena	3.040	57.90	64.63				
Base Kaena	3.110	59.30	66.03				
Top Mammoth	3.220	61.20	67.93				
Base Mammoth	3.330			61.63	70.36		
Gauss/Gilbert	3.580	66.80	74.54	65.70	74.43	67.18	75.30
Top Cochiti	4.180	70.50	78.24	68.78	77.51	69.25	77.37
Base Gilbert	5.890	89.50	97.64	88.35	97.65	88.63	97.68
Base 3An.1n	6.140	92.25	100.39			91.75	101.33
Top 3An.2n	6.270	93.30	101.72			92.37	101.95
Top 3Ar	6.570	96.40	104.82			96.30	105.88
Top 5n.2n	9.920	111.80	120.89	110.87	121.38	110.70	120.81
Base 5n.2n	10.950	129.70	140.20	128.13	140.12	128.67	140.15
Base 5r	11.940	141.85	154.11	141.27	154.02	140.63	153.94
Base 5An.1n	12.080						
Top 5An.2n	12.180						
Base 5An.2n	12.400	145.65	157.91	146.32	159.84	144.73	158.04
Base 5Ar	12.990	159.60	172.54	160.87	176.07	160.83	175.89
Base 5AAn	13.139	165.50	180.18	165.37	181.84	166.67	181.73
Top 5ABn	13.302	168.00	182.68	167.49	186.96	167.65	184.43
Base 5ABn	13.510	181.35	199.31	181.32	199.37	182.07	199.55
Top 5ACn	13.703	187.85	205.81	188.29	206.70	189.20	207.95

Note: Mat. = Matuyama, * = affected by dropstone.

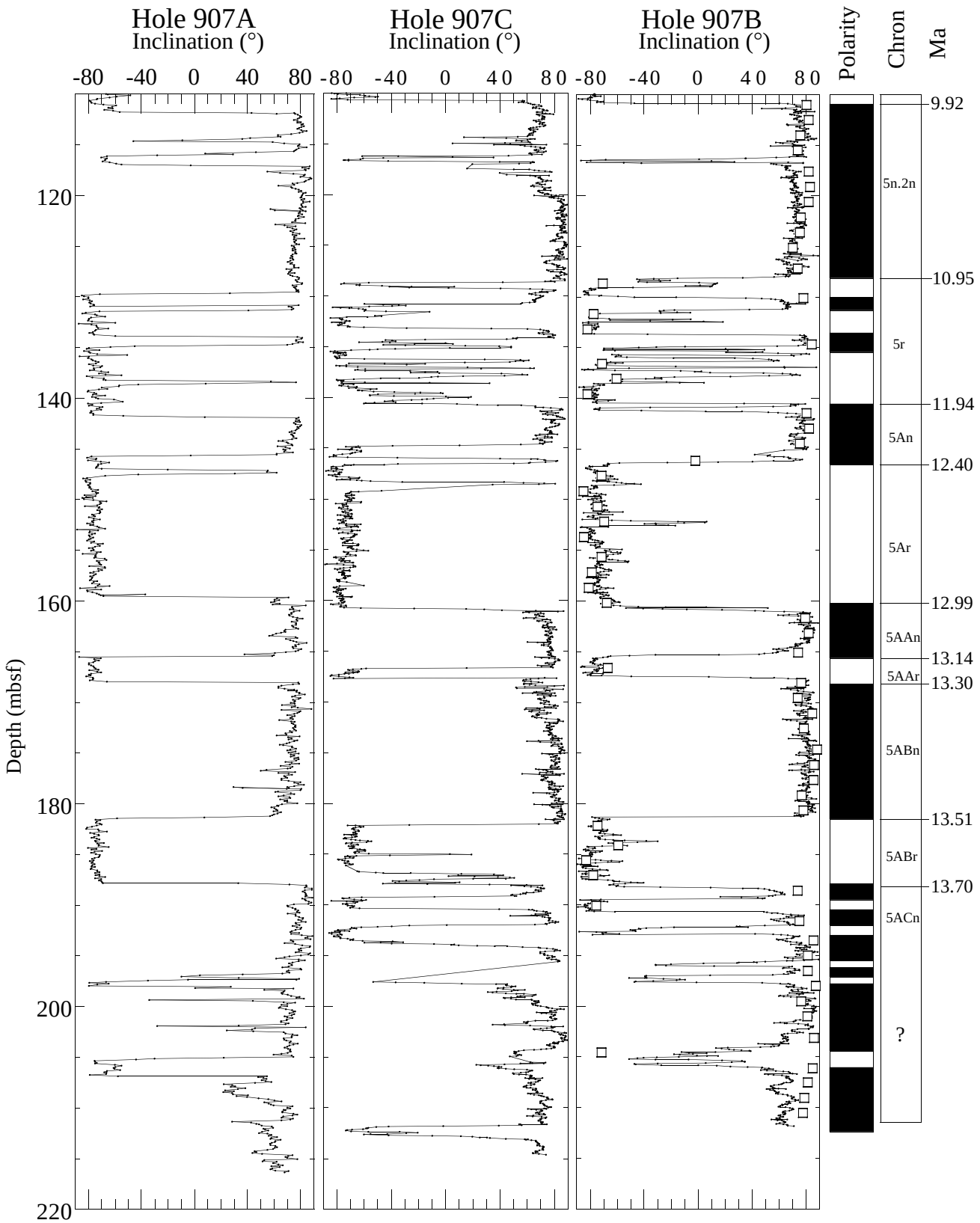

Figure 5. Shipboard (pass-through magnetometer) inclination data after AF demagnetization at peak fields of 30 mT for Hole 907A, and 25 mT for Holes 907B and 907C, in the 110–215 mbsf interval. Open squares indicate component inclinations determined from discrete (7 cm^3) samples measured postcruise. Component directions were computed from orthogonal projections of AF demagnetization data. Hole 907A data are from Leg 151 (Shipboard Scientific Party, 1995). Absolute ages of polarity chron boundaries are from Cande and Kent (1995).

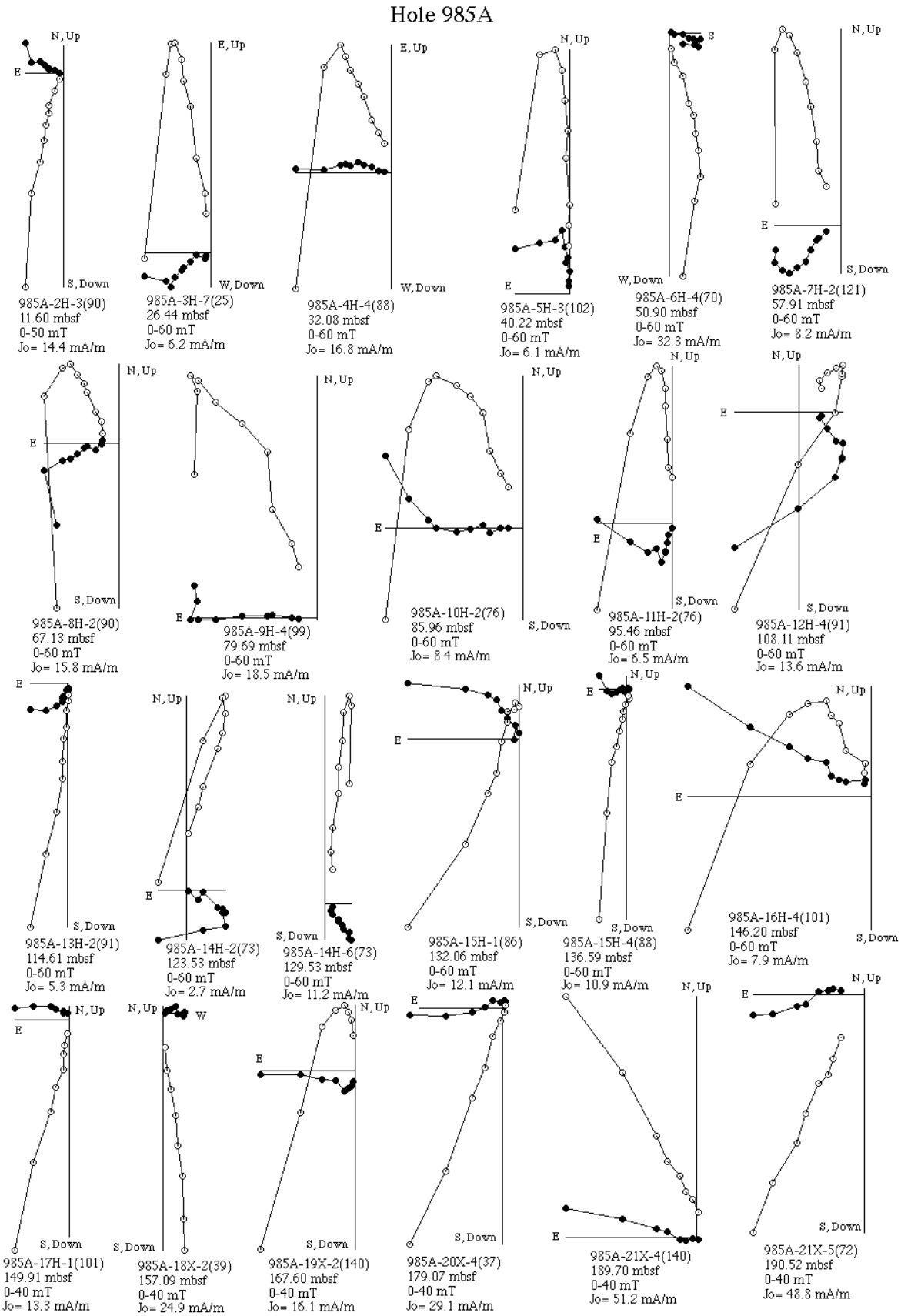

Figure 6. Orthogonal projection of AF demagnetization data from discrete samples in the 0–200 mbsf interval of Hole 985A. Open and solid symbols indicate projections on the vertical and horizontal planes, respectively. Symbols and abbreviations as in Figure 2.

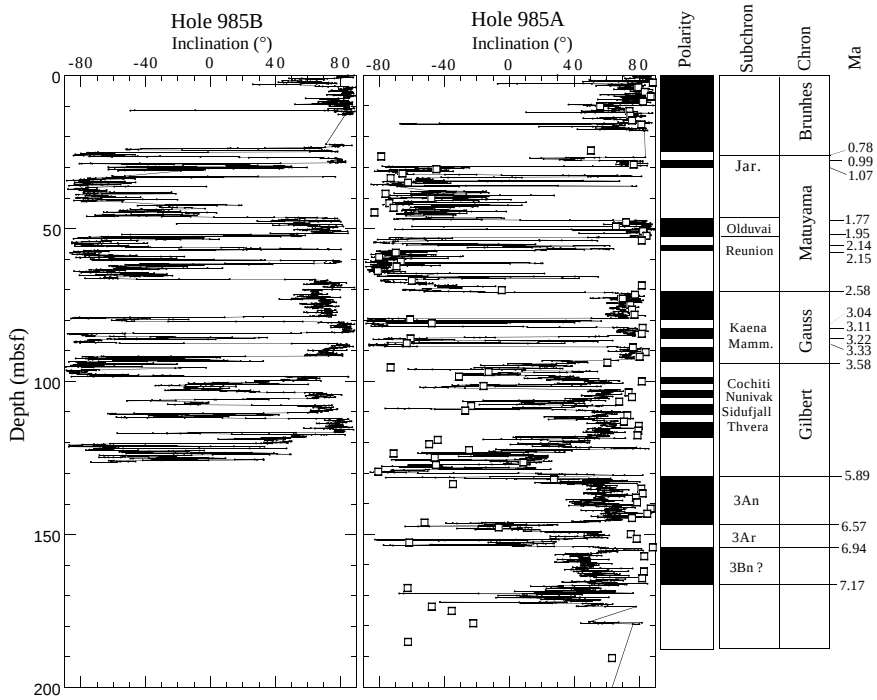

Figure 7. Shipboard (pass-through magnetometer) inclination data after AF demagnetization at peak fields of 25 mT for Holes 985A and 985B, in the 0–180 mbsf interval. Open squares indicate component inclinations determined from discrete (7 cm^3) samples measured postcruise. Component directions were computed from orthogonal projections of AF demagnetization data. Absolute ages of polarity chron boundaries are from Cande and Kent (1995).

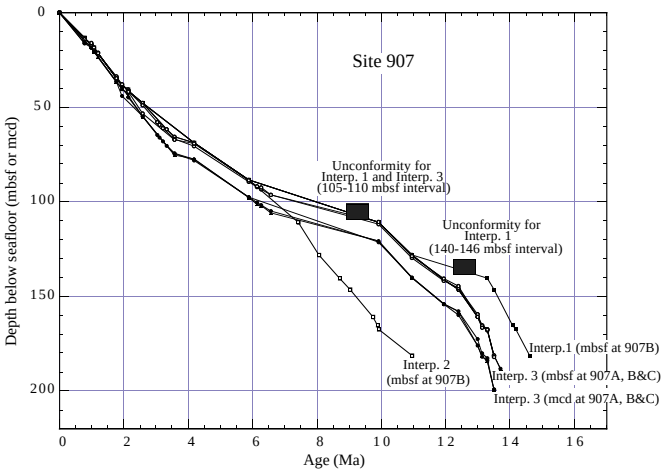

Figure 8. Age-depth plot for the various interpretations (Interp.) of the Site 907 magnetic stratigraphy. Interpretations 1 and 2 are from the Leg 162 *Initial Reports* volume (Shipboard Scientific Party, 1996a). Interpretation 1 follows the original Leg 151 interpretation at Hole 907A (Shipboard Scientific Party, 1995). Interpretation 3 (this paper) is very similar to that proposed by Koç and Scherer (1996) in their reinterpretation of Hole 907A. Absolute ages of polarity chron boundaries are from Cande and Kent (1995).

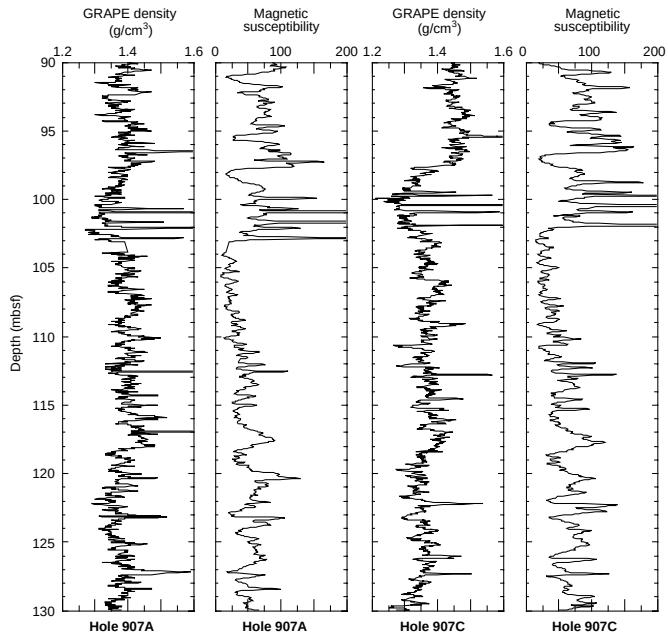

Figure 9. GRAPE density and magnetic susceptibility from 90 mbsf to 130 mbsf in Holes 907A and 907C (Shipboard Scientific Party, 1995, 1996a). Discrete ash layers are identified by sharp peaks in GRAPE density and magnetic susceptibility; dispersed ash zones have more subtle expressions using these parameters (Rack et al., 1996). The low-susceptibility zone in each hole between 107 and 103 mbsf is associated with several diatom last appearance datums, suggesting one or more apparent hiatuses in sedimentation within this interval (Koç and Scherer, 1996). Susceptibility values should be multiplied by 0.63×10^{-5} to convert to SI units of volume susceptibility.

four diatom species—*Coscinodiscus norwegicus*, *Cymatostra biharensis*, *Denticulopsis hustedtii*, and *Ikebea tenuis*—have their last occurrences at in the 113–115 mbsf interval at Hole 907A. As noted by Koç and Scherer (1996), this juxtaposition of last occurrences implies a hiatus at this level.

Site 985

The polarity chron interpretation at Site 985 (Fig. 7; Table 3) is not aided by biostratigraphic constraints because of the absence of useful biostratigraphic datums at this site (Shipboard Scientific Party, 1996c). Natural gamma data from the shipboard multisensor track

Table 3. Polarity chron boundaries at Site 985.

Polarity chron boundary	Age (Ma)	Hole 985A Depth (mbsf)	Hole 985A Depth (mcd)	Hole 985B Depth (mbsf)	Hole 985B Depth (mcd)
Brunhes/Mat.	0.78	25.45	26.12	25.05	27.21
Top Jaramillo	0.99	27.80	29.17	26.67	28.83
Base Jaramillo	1.07	29.70	31.07	28.67	30.83
Top Olduvai	1.77	47.25	49.72	46.25	49.66
Base Olduvai	1.95	53.03	55.50	52.67	56.62
Top Reunion	2.13	55.65	59.56	56.25	60.20
Base Reunion	2.14	57.20	61.11	57.10	61.05
Mat./Gauss	2.58	70.90	75.61	66.60	72.03
Top Kaena	3.04	79.37	84.29	79.03	84.29
Base Kaena	3.11	82.13	87.05	80.37	87.02
Top Mammoth	3.22	85.53	91.07	84.23	90.88
Base Mammoth	3.33	88.67	94.21	87.57	94.22
Gauss/Gilbert	3.58	93.30	99.64	91.77	98.88
Top Cochiti	4.18			98.40	105.50
Base Cochiti	4.29			100.40	107.41
Top Nunivak	4.48			103.60	110.61
Base Nunivak	4.62			105.95	112.96
Top Sidjufjall	4.80			107.67	114.68
Base Sidjufjall	4.89			110.38	119.02
Top Thvera	4.98			111.98	120.62
Base Thvera	5.23			116.82	125.64
Base Gilbert	5.89	131.95	139.79		
Base 3An.1n	6.14				
Top 3An.2n	6.27				
Top 3Ar	6.57	146.10	153.94		
Base 3Ar	6.94	154.00	161.84		

Note: Mat. = Matuyama.

provide a means of correlating Site 985 with Site 907 (Fig. 10), providing corroboration for the magnetostratigraphic interpretations down to the base Gilbert Chron. The age-depth plot based on these interpretations indicates fairly constant sedimentation rates to ~160 mbsf (Fig. 11). No magnetostratigraphic interpretation is possible below this level because of drilling-related deformation of the core.

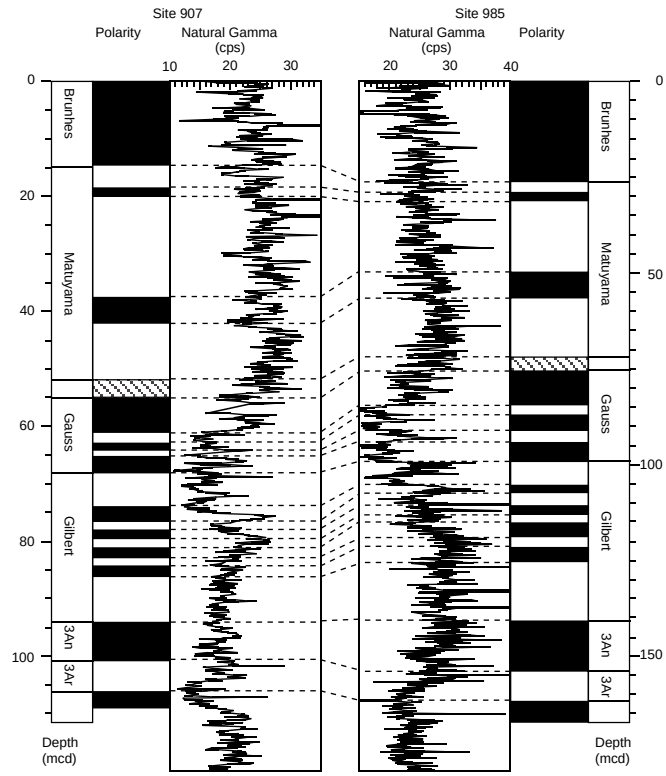

Figure 10. Natural gamma data from the shipboard multisensor track (Shipboard Scientific Party, 1996a) used to correlate the upper parts of the sections from Sites 907 and 985.

CONCLUSIONS

The upper Miocene–Pleistocene sections at Sites 907 and 985 have provided the most complete magnetostratigraphic records available from the Norwegian-Greenland Sea. Although the sections are not affected by unconformities to the same extent as the Leg 104 (Vøring Plateau) sites, the interpretation of the magnetic stratigraphies is not unequivocal. Siliceous microfossils are reasonably well preserved at Site 907; however, the lack of cosmopolitan biostratigraphic markers indicates that the magnetostratigraphic interpretations cannot be easily ratified by biomagnetostratigraphic correlations from outside the area.

We use silicoflagellate datums at Site 907 to "pin" the magnetostratigraphic interpretations. Silicoflagellate datums at Site 982 (North Atlantic) and DSDP Leg 408 can be tied to nannofossil zones, which in turn can be tied to the polarity time scale. The resulting magnetostratigraphic interpretation at Site 907 implies a hiatus at ~105–110 mbsf where deposition was halted or very slow for ~2.7 m.y. in the 7.2–9.9 Ma interval. Apart from this unconformity, sedimentation rates were fairly constant at Site 907 with an increase in sedimentation rate at ~12 Ma. At Site 985, the magnetostratigraphic record does not extend beyond ~6 Ma. Sedimentation rates appear to have been fairly constant since that time.

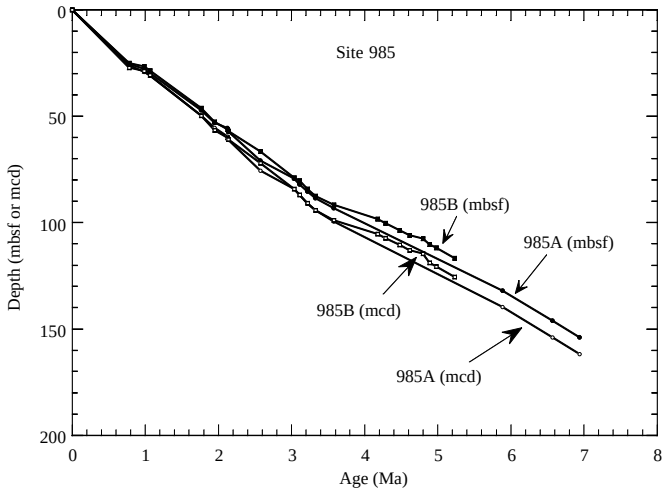

Figure 11. Age-depth plot for Site 985 magnetic stratigraphy. Absolute ages of polarity chron boundaries are from Cande and Kent (1995).

ACKNOWLEDGMENTS

We thank C. Kissel and C. Laj for logistical support, K. Huang for laboratory assistance, and U. Bleil for a review of the manuscript. The paleomagnetic laboratory at Gif-sur-Yvette is supported by CEA and CNRS. At the University of Florida, this project was supported by the U.S. Science Support Program, LSCE contribution 34.

REFERENCES

Barron, J.A., and Gladenkov, A.Y., 1995. Early Miocene to Pleistocene diatom stratigraphy of Leg 145. *In* Rea, D.K., Basov, I.A., Scholl, D.W., and Allan, J.F. (Eds.), *Proc. ODP, Sci. Results*, 145: College Station, TX (Ocean Drilling Program), 3–19.

Berggren, W.A., Kent, D.V., Swisher, C.C., III, and Aubry, M.-P., 1995. A revised Cenozoic geochronology and chronostratigraphy. *In* Berggren, W.A., Kent, D.V., Aubry, M.-P., and Hardenbol, J. (Eds.), *Geochronol-*

ogy, Time Scales and Global Stratigraphic Correlation. Spec. Publ.—Soc. Econ. Paleontol. Mineral. (Soc. Sediment. Geol.), 54:129–212.

Bukry, D., 1979. Coccolith and silicoflagellate stratigraphy, northern Mid-Atlantic Ridge and Reykjanes Ridge, Deep Sea Drilling Project Leg 49. *In* Luyendyk, B.P., Cann, J.R., et al., *Init. Repts. DSDP,* 49: Washington (U.S. Govt. Printing Office), 551–581.

Cande, S.C., and Kent, D.V., 1995. Revised calibration of the geomagnetic polarity timescale for the Late Cretaceous and Cenozoic. *J. Geophys. Res.,* 100:6093–6095.

Fronval, T., and Jansen, E., 1996. Late Neogene paleoclimates and paleoceanography in the Iceland-Norwegian Sea: evidence from the Iceland and Vøring Plateaus. *In* Thiede, J., Myhre, A.M., Firth, J.V., Johnson, G.L., and Ruddiman, W.F. (Eds.), *Proc. ODP, Sci. Results,* 151: College Station, TX (Ocean Drilling Program), 455–468.

Hagelberg, T., Shackleton, N., Pisias, N., and Shipboard Scientific Party, 1992. Development of composite depth sections for Sites 844 through 854. *In* Mayer, L., Pisias, N., Janecek, T., et al., *Proc. ODP, Init. Repts.,* 138 (Pt. 1): College Station, TX (Ocean Drilling Program), 79–85.

Heinrich, R., and Baumann, K.H., 1994. Evolution of the Norwegian Current and the Scandinavian Ice Sheets during the past 2.6 m.y.: evidence from ODP Leg 104 biogenic carbonate and terrigenous records. *Palaeogeogr., Palaeoclimatol., Palaeoecol.,* 108:75–94.

Jansen, E., Raymo, M.E., Blum, P., et al., 1996. *Proc. ODP, Init. Repts.,* 162: College Station, TX (Ocean Drilling Program).

Kirschvink, J.L., 1980. The least-squares line and plane and the analysis of palaeomagnetic data. *Geophys. J. R. Astron. Soc.,* 62:699–718.

Koç, N., and Scherer, R.P., 1996. Neogene diatom biostratigraphy of the Iceland Sea Site 907. *In* Thiede, J., Myhre, A.M., Firth, J.V., Johnson, G.L., and Ruddiman, W.F. (Eds.), *Proc. ODP, Sci. Results,* 151: College Station, TX (Ocean Drilling Program), 61–70.

Lacasse, C., Paterne, M., Werver, R., Wallrabe-Adams, H.-J., Sigurdsson, H., Carey, S., and Pinte, G., 1996. Geochemistry and origin of Pliocene and Pleistocene ash layers from the Iceland Plateau, Site 907. *In* Thiede, J., Myhre, A.M., Firth, J.V., Johnson, G.L., and Ruddiman, W.F. (Eds.), *Proc. ODP, Sci. Results,* 151: College Station, TX (Ocean Drilling Program), 309–331.

Locker, S., and Martini, E., 1989. Cenozoic silicoflagellates, ebridians, and actiniscidians from the Vøring Plateau (ODP Leg 104). *In* Eldholm, O., Thiede, J., Taylor, E., et al., *Proc. ODP, Sci. Results,* 104: College Station, TX (Ocean Drilling Program), 543–585.

Okada, H., and Bukry, D., 1980. Supplementary modification and introduction of code numbers to the low-latitude coccolith biostratigraphic zonation (Bukry, 1973; 1975). *Mar. Micropaleontol.,* 5:321–325.

Rack, F.R., Bloemendal, J., Wolf-Welling, T.C.W., O'Connell, S., Cremer, M., Winkler, A., Thiede, J., Black, K., and Hood, H., 1996. Development of physical properties relationships, interhole composite depth profiles, and sedimentologic ground truthing of multi-sensor core measurements: a synthesis of results. *In* Thiede, J., Myhre, A.M., Firth, J.V., Johnson, G.L., and Ruddiman, W.F. (Eds.), *Proc. ODP, Sci. Results,* 151: College Station, TX (Ocean Drilling Program), 595–626.

Shipboard Scientific Party, 1995. Site 907. *In* Myhre, A.M., Thiede, J., Firth, J.V., et al., *Proc. ODP, Init. Repts.,* 151: College Station, TX (Ocean Drilling Program), 57–111.

————, 1996a. Site 907 (revisited). *In* Jansen, E., Raymo, M.E., Blum, P., et al., *Proc. ODP, Init. Repts.,* 162: College Station, TX (Ocean Drilling Program), 223–252.

————, 1996b. Site 982. *In* Jansen, E., Raymo, M.E., Blum, P., et al., *Proc. ODP, Init. Repts.,* 162: College Station, TX (Ocean Drilling Program), 91–138.

————, 1996c. Site 985. *In* Jansen, E., Raymo, M.E., Blum, P., et al., *Proc. ODP, Init. Repts.,* 162: College Station, TX (Ocean Drilling Program), 253–285.

Talwani, M., and Eldholm, O., 1977. Evolution of the Norwegian-Greenland Sea. *Geol. Soc. Am. Bull.,* 88:969–999.

Werner, R., Wallrabe-Adams, H.-J., Lacasse, C., Schmincke, H.-U., and Thiede, J., 1996. Distribution, chemical composition, and sources of Oligocene to Miocene volcanic ashes from Sites 907, 908, and 913. *In* Thiede, J., Myhre, A.M., Firth, J.V., Johnson, G.L., and Ruddiman, W.F. (Eds.), *Proc. ODP, Sci. Results,* 151: College Station, TX (Ocean Drilling Program), 333–350.

Date of initial receipt: 10 September 1997
Date of acceptance: 25 March 1998
Ms 162SR-036

APPENDIX A
Revised composite depths, Site 907.

Core, section, interval (cm)	Depth mbsf	Depth mcd	Depth mcd – mbsf
162-907A-			
1H-1, 150	0.00	0.00	0.00
1H-2, 150	1.50	1.50	0.00
1H-3, 150	3.00	3.00	0.00
1H-4, 150	4.50	4.50	0.00
1H-5, 100	6.00	6.00	0.00
1H-CC, 27	7.00	7.00	0.00
2H-1, 150	7.30	7.33	0.03
2H-2, 150	8.80	8.83	0.03
2H-3, 150	10.30	10.33	0.03
2H-4, 150	11.80	11.83	0.03
2H-5, 150	13.30	13.33	0.03
2H-6, 150	14.80	14.83	0.03
2H-7, 56	16.30	16.33	0.03
2H-CC, 25	16.86	16.89	0.03
3H-1, 150	16.80	18.30	1.50
3H-2, 150	18.30	19.80	1.50
3H-3, 150	19.80	21.30	1.50
3H-4, 150	21.30	22.80	1.50
3H-5, 150	22.80	24.30	1.50
3H-6, 150	24.30	25.80	1.50
3H-7, 46	25.80	27.30	1.50
3H-CC, 40	26.26	27.76	1.50
4H-1, 150	26.30	29.03	2.73
4H-2, 150	27.80	30.53	2.73
4H-3, 150	29.30	32.03	2.73
4H-4, 150	30.80	33.53	2.73
4H-5, 150	32.30	35.03	2.73
4H-6, 150	33.80	36.53	2.73
4H-7, 73	35.30	38.03	2.73
4H-CC, 20	36.03	38.76	2.73
5H-1, 150	35.80	41.75	5.95
5H-2, 150	37.30	43.25	5.95
5H-3, 150	38.80	44.75	5.95
5H-4, 150	40.30	46.25	5.95
5H-5, 150	41.80	47.75	5.95
5H-6, 150	43.30	49.25	5.95
5H-7, 85	44.80	50.75	5.95
5H-CC, 25	45.65	51.60	5.95
6H-1, 150	45.30	51.09	5.79
6H-2, 150	46.80	52.59	5.79
6H-3, 150	48.30	54.09	5.79
6H-4, 150	49.80	55.59	5.79
6H-5, 150	51.30	57.09	5.79
6H-6, 150	52.80	58.59	5.79
6H-7, 71	54.30	60.09	5.79
6H-CC, 35	55.01	60.80	5.79
7H-1, 150	54.80	61.53	6.73
7H-2, 150	56.30	63.03	6.73
7H-3, 150	57.80	64.53	6.73
7H-4, 150	59.30	66.03	6.73
7H-5, 150	60.80	67.53	6.73
7H-6, 150	62.30	69.03	6.73
7H-7, 64	63.80	70.53	6.73
7H-CC, 26	64.44	71.17	6.73
8H-1, 150	64.30	72.04	7.74
8H-2, 150	65.80	73.54	7.74
8H-3, 150	67.30	75.04	7.74
8H-4, 150	68.80	76.54	7.74
8H-5, 150	70.30	78.04	7.74
8H-6, 150	71.80	79.54	7.74
8H-7, 55	73.30	81.04	7.74
8H-CC, 27	73.85	81.59	7.74
9H-1, 150	73.80	81.46	7.66
9H-2, 150	75.30	82.96	7.66
9H-3, 150	76.80	84.46	7.66
9H-4, 150	78.30	85.96	7.66
9H-5, 150	79.80	87.46	7.66
9H-6, 150	81.30	88.96	7.66
9H-7, 81	82.80	90.46	7.66
9H-CC, 38	83.61	91.27	7.66
10H-1, 150	83.30	91.44	8.14
10H-2, 150	84.80	92.94	8.14
10H-3, 150	86.30	94.44	8.14
10H-4, 150	87.80	95.94	8.14
10H-5, 150	89.30	97.44	8.14
10H-6, 150	90.80	98.94	8.14
10H-7, 71	92.30	100.44	8.14
10H-CC, 26	93.01	101.15	8.14
11H-1, 150	92.80	101.22	8.42
11H-2, 150	94.30	102.72	8.42
11H-3, 150	95.80	104.22	8.42
11H-4, 150	97.30	105.72	8.42
11H-5, 150	98.80	107.22	8.42
11H-6, 150	100.30	108.72	8.42
11H-7, 84	101.80	110.22	8.42
11H-CC, 23	102.64	111.06	8.42
12H-1, 150	102.30	111.39	9.09
12H-2, 150	103.80	112.89	9.09

APPENDIX A (continued).

Core, section, interval (cm)	Depth mbsf	Depth mcd	mcd – mbsf
12H-3, 150	105.30	114.39	9.09
12H-4, 150	106.80	115.89	9.09
12H-5, 150	108.30	117.39	9.09
12H-6, 150	109.80	118.89	9.09
12H-7, 67	111.30	120.39	9.09
12H-CC, 30	111.97	121.06	9.09
13H-1, 150	111.80	122.71	10.91
13H-2, 150	113.30	124.21	10.91
13H-3, 150	114.80	125.71	10.91
13H-4, 150	116.30	127.21	10.91
13H-5, 150	117.80	128.71	10.91
13H-6, 150	119.30	130.21	10.91
13H-7, 82	120.80	131.71	10.91
13H-CC, 18	121.62	132.53	10.91
14H-1, 150	121.30	131.80	10.50
14H-2, 150	122.80	133.30	10.50
14H-3, 150	124.30	134.80	10.50
14H-4, 150	125.80	136.30	10.50
14H-5, 150	127.30	137.80	10.50
14H-6, 150	128.80	139.30	10.50
14H-7, 68	130.30	140.80	10.50
14H-CC, 25	130.98	141.48	10.50
15H-1, 150	130.80	142.60	11.80
15H-2, 150	132.30	144.10	11.80
15H-3, 150	133.80	145.60	11.80
15H-4, 150	135.30	147.10	11.80
15H-5, 153	136.80	148.60	11.80
15H-6, 150	138.33	150.13	11.80
15H-7, 42	139.83	151.63	11.80
15H-CC, 28	140.25	152.05	11.80
16H-1, 150	140.30	152.56	12.26
16H-2, 150	141.80	154.06	12.26
16H-3, 150	143.30	155.56	12.26
16H-4, 150	144.80	157.06	12.26
16H-5, 150	146.30	158.56	12.26
16H-6, 150	147.80	160.06	12.26
16H-7, 61	149.30	161.56	12.26
16H-CC, 31	149.91	162.17	12.26
17H-1, 150	149.80	162.74	12.94
17H-2, 150	151.30	164.24	12.94
17H-3, 150	152.80	165.74	12.94
17H-4, 150	154.30	167.24	12.94
17H-5, 150	155.80	168.74	12.94
17H-6, 150	157.30	170.24	12.94
17H-7, 74	158.80	171.74	12.94
17H-CC, 27	159.54	172.48	12.94
18H-1, 150	159.30	173.98	14.68
18H-2, 150	160.80	175.48	14.68
18H-3, 150	162.30	176.98	14.68
18H-4, 150	163.80	178.48	14.68
18H-5, 150	165.30	179.98	14.68
18H-6, 150	166.80	181.48	14.68
18H-7, 60	168.30	182.98	14.68
18H-CC, 27	168.90	183.58	14.68
19H-1, 150	168.80	186.23	17.43
19H-2, 150	170.30	187.73	17.43
19H-3, 150	171.80	189.23	17.43
19H-4, 150	173.30	190.73	17.43
19H-5, 150	174.80	192.23	17.43
19H-6, 150	176.30	193.73	17.43
19H-7, 75	177.80	195.23	17.43
19H-CC, 24	178.55	195.98	17.43
20H-1, 150	178.30	196.26	17.96
20H-2, 150	179.80	197.76	17.96
20H-3, 150	181.30	199.26	17.96
20H-4, 150	182.80	200.76	17.96
20H-5, 150	184.30	202.26	17.96
20H-6, 150	185.80	203.76	17.96
20H-7, 60	187.30	205.26	17.96
20H-CC, 25	187.90	205.86	17.96
21H-1, 150	187.80	207.22	19.42
21H-2, 150	189.30	208.72	19.42
21H-3, 150	190.80	210.22	19.42
21H-4, 150	192.30	211.72	19.42
21H-5, 150	193.80	213.22	19.42
21H-6, 150	195.30	214.72	19.42
21H-7, 58	196.80	216.22	19.42
21H-CC, 1	197.38	216.80	19.42
22H-1, 150	197.30	216.83	19.53
22H-2, 150	198.80	218.33	19.53
22H-3, 150	200.30	219.83	19.53
22H-4, 150	201.80	221.33	19.53
22H-5, 150	203.30	222.83	19.53
22H-6, 150	204.80	224.33	19.53
22H-7, 55	206.30	225.83	19.53
22H-CC, 3	206.85	226.38	19.53
23H-1, 150	206.80	226.20	19.40
23H-2, 150	208.30	227.70	19.40
23H-3, 150	209.80	229.20	19.40
23H-4, 150	211.30	230.70	19.40
23H-5, 150	212.80	232.20	19.40
23H-6, 150	214.30	233.70	19.40
23H-7, 60	215.80	235.20	19.40
23H-CC, 18	216.40	235.80	19.40
24X-CC, 53	216.30	235.70	19.40
25X-1, 138	217.30	236.70	19.40
25X-2, 150	218.68	238.08	19.40
25X-3, 23	220.18	239.58	19.40
26X-1, 144	221.00	240.40	19.40
26X-2, 92	222.44	241.84	19.40
162-907B-			
1H-1, 150	0.00	0.22	0.22
1H-2, 100	1.50	1.72	0.22
1H-CC, 17	2.50	2.72	0.22
2H-1, 150	2.70	3.03	0.33
2H-2, 150	4.20	4.53	0.33
2H-3, 150	5.70	6.03	0.33
2H-4, 150	7.20	7.53	0.33
2H-5, 150	8.70	9.03	0.33
2H-6, 150	10.20	10.53	0.33
2H-7, 73	11.70	12.03	0.33
2H-CC, 28	12.43	12.76	0.33
3H-1, 150	12.20	13.77	1.57
3H-2, 150	13.70	15.27	1.57
3H-3, 150	15.20	16.77	1.57
3H-4, 150	16.70	18.27	1.57
3H-5, 150	18.20	19.77	1.57
3H-6, 150	19.70	21.27	1.57
3H-7, 70	21.20	22.77	1.57
3H-CC, 20	21.90	23.47	1.57
4H-1, 150	21.70	23.85	2.15
4H-2, 150	23.20	25.35	2.15
4H-3, 150	24.70	26.85	2.15
4H-4, 150	26.20	28.35	2.15
4H-5, 150	27.70	29.85	2.15
4H-6, 150	29.20	31.35	2.15
4H-7, 63	30.70	32.85	2.15
4H-CC, 25	31.33	33.48	2.15
5H-1, 150	31.20	33.18	1.98
5H-2, 150	32.70	34.68	1.98
5H-3, 150	34.20	36.18	1.98
5H-4, 150	35.70	37.68	1.98
5H-5, 150	37.20	39.18	1.98
5H-6, 150	38.70	40.68	1.98
5H-7, 68	40.20	42.18	1.98
5H-CC, 24	40.88	42.86	1.98
6H-1, 150	40.70	43.95	3.25
6H-2, 150	42.20	45.45	3.25
6H-3, 150	43.70	46.95	3.25
6H-4, 150	45.20	48.45	3.25
6H-5, 150	46.70	53.64	6.94
6H-6, 150	48.20	55.14	6.94
6H-7, 64	49.70	56.64	6.94
6H-CC, 31	50.34	57.28	6.94
7H-1, 150	50.20	58.38	8.18
7H-2, 150	51.70	59.88	8.18
7H-3, 150	53.20	61.38	8.18
7H-4, 150	54.70	62.88	8.18
7H-5, 150	56.20	64.38	8.18
7H-6, 150	57.70	65.88	8.18
7H-7, 70	59.20	67.38	8.18
7H-CC, 25	59.90	68.08	8.18
8H-1, 150	59.70	68.43	8.73
8H-2, 150	61.20	69.93	8.73
8H-3, 150	62.70	71.43	8.73
8H-4, 150	64.20	72.93	8.73
8H-5, 150	65.70	74.43	8.73
8H-6, 150	67.20	75.93	8.73
8H-7, 56	68.70	77.43	8.73
8H-CC, 23	69.26	77.99	8.73
9H-1, 150	69.20	78.36	9.16
9H-2, 150	70.70	79.86	9.16
9H-3, 150	72.20	81.36	9.16
9H-4, 150	73.70	82.86	9.16
9H-5, 150	75.20	84.36	9.16
9H-6, 150	76.70	85.86	9.16
9H-7, 55	78.20	87.36	9.16
9H-CC, 24	78.75	87.91	9.16
10H-1, 150	78.70	88.00	9.30
10H-2, 150	80.20	89.50	9.30
10H-3, 150	81.70	91.00	9.30
10H-4, 150	83.20	92.50	9.30
10H-5, 150	84.70	94.00	9.30
10H-6, 150	86.20	95.50	9.30
10H-7, 60	87.70	97.00	9.30
10H-CC, 22	88.30	97.60	9.30
11H-1, 150	88.20	98.11	9.91
11H-2, 150	89.70	99.61	9.91
11H-3, 150	91.20	101.11	9.91

APPENDIX A (continued).

Core, section, interval (cm)	Depth mbsf	Depth mcd	Depth mcd – mbsf
11H-4, 150	92.70	102.61	9.91
11H-5, 150	94.20	104.11	9.91
11H-6, 150	95.70	105.61	9.91
11H-7, 50	97.20	107.11	9.91
11H-CC, 23	97.70	107.61	9.91
12H-1, 150	97.70	107.54	9.84
12H-2, 150	99.20	109.04	9.84
12H-3, 150	100.70	110.54	9.84
12H-4, 150	102.20	112.04	9.84
12H-5, 150	103.70	113.54	9.84
12H-6, 150	105.20	115.04	9.84
12H-7, 62	106.70	116.54	9.84
12H-CC, 23	107.32	117.16	9.84
13H-1, 150	107.20	117.71	10.51
13H-2, 150	108.70	119.21	10.51
13H-3, 150	110.20	120.71	10.51
13H-4, 150	111.70	122.21	10.51
13H-5, 150	113.20	123.71	10.51
13H-6, 150	114.70	125.21	10.51
13H-7, 64	116.20	126.71	10.51
13H-CC, 24	116.84	127.35	10.51
14H-1, 150	116.70	128.37	11.67
14H-2, 150	118.20	129.87	11.67
14H-3, 150	119.70	131.37	11.67
14H-4, 150	121.20	132.87	11.67
14H-5, 150	122.70	134.37	11.67
14H-6, 150	124.20	135.87	11.67
14H-7, 74	125.70	137.37	11.67
14H-CC, 25	126.44	138.11	11.67
15H-1, 150	126.20	138.19	11.99
15H-2, 150	127.70	139.69	11.99
15H-3, 150	129.20	141.19	11.99
15H-4, 150	130.70	142.69	11.99
15H-5, 150	132.20	144.19	11.99
15H-6, 150	133.70	145.69	11.99
15H-7, 60	135.20	147.19	11.99
15H-CC, 24	135.80	147.79	11.99
16H-1, 150	135.70	148.45	12.75
16H-2, 150	137.20	149.95	12.75
16H-3, 150	138.70	151.45	12.75
16H-4, 42	140.20	152.95	12.75
16H-5, 150	140.62	153.37	12.75
16H-6, 150	142.12	154.87	12.75
16H-7, 150	143.62	156.37	12.75
16H-CC, 24	145.12	157.87	12.75
17H-1, 150	145.20	158.72	13.52
17H-2, 150	146.70	160.22	13.52
17H-3, 150	148.20	161.72	13.52
17H-4, 150	149.70	163.22	13.52
17H-5, 150	151.20	164.72	13.52
17H-6, 150	152.70	166.22	13.52
17H-7, 64	154.20	167.72	13.52
17H-CC, 25	154.84	168.36	13.52
18H-1, 150	154.70	169.90	15.20
18H-2, 150	156.20	171.40	15.20
18H-3, 150	157.70	172.90	15.20
18H-4, 150	159.20	174.40	15.20
18H-5, 150	160.70	175.90	15.20
18H-6, 150	162.20	177.40	15.20
18H-7, 61	163.70	178.90	15.20
18H-CC, 13	164.31	179.51	15.20
19H-1, 150	164.20	180.67	16.47
19H-2, 150	165.70	182.17	16.47
19H-3, 150	167.20	183.67	16.47
19H-4, 150	168.70	185.17	16.47
19H-5, 150	170.20	186.67	16.47
19H-6, 150	171.70	188.17	16.47
19H-7, 68	173.20	189.67	16.47
19H-CC, 25	173.88	190.35	16.47
20H-1, 150	173.70	191.75	18.05
20H-2, 150	175.20	193.25	18.05
20H-3, 150	176.70	194.75	18.05
20H-4, 150	178.20	196.25	18.05
20H-5, 150	179.70	197.75	18.05
20H-6, 150	181.20	199.25	18.05
20H-7, 56	182.70	200.75	18.05
20H-CC, 25	183.26	201.31	18.05
21H-1, 150	183.20	201.61	18.41
21H-2, 150	184.70	203.11	18.41
21H-3, 150	186.20	204.61	18.41
21H-4, 150	187.70	206.11	18.41
21H-5, 150	189.20	207.61	18.41
21H-6, 150	190.70	209.11	18.41
21H-7, 79	192.20	210.61	18.41
21H-CC, 24	192.99	211.40	18.41
22H-1, 150	192.70	212.77	20.07
22H-2, 150	194.20	214.27	20.07
22H-3, 150	195.70	215.77	20.07
22H-4, 150	197.20	217.27	20.07
22H-5, 150	198.70	218.77	20.07
22H-6, 150	200.20	220.27	20.07
22H-7, 44	201.70	221.77	20.07
22H-CC, 21	202.14	222.21	20.07
23H-1, 150	202.20	223.00	20.80
23H-2, 150	203.70	224.50	20.80
23H-3, 150	205.20	226.00	20.80
23H-4, 150	206.70	227.50	20.80
23H-5, 150	208.20	229.00	20.80
23H-6, 150	209.70	230.50	20.80
23H-7, 65	211.20	232.00	20.80
23H-CC, 23	211.85	232.65	20.80
162-907C-			
1H-1, 150	0.00	0.00	0.00
1H-2, 150	1.50	1.50	0.00
1H-3, 150	3.00	3.00	0.00
1H-4, 140	4.50	4.50	0.00
1H-CC, 20	5.90	5.90	0.00
2H-1, 150	6.10	6.96	0.86
2H-2, 150	7.60	8.46	0.86
2H-3, 150	9.10	9.96	0.86
2H-4, 150	10.60	11.46	0.86
2H-5, 150	12.10	12.96	0.86
2H-6, 150	13.60	14.46	0.86
2H-7, 56	15.10	15.96	0.86
2H-CC, 23	15.66	16.52	0.86
3H-1, 150	15.60	17.79	2.19
3H-2, 150	17.10	19.29	2.19
3H-3, 150	18.60	20.79	2.19
3H-4, 150	20.10	22.29	2.19
3H-5, 150	21.60	23.79	2.19
3H-6, 88	23.10	25.29	2.19
3H-CC, 26	23.98	26.17	2.19
4H-1, 150	25.10	27.05	1.95
4H-2, 150	26.60	28.55	1.95
4H-3, 150	28.10	30.05	1.95
4H-4, 150	29.60	31.55	1.95
4H-5, 150	31.10	33.05	1.95
4H-6, 150	32.60	34.55	1.95
4H-7, 70	34.10	36.05	1.95
4H-CC, 21	34.80	36.75	1.95
5H-1, 150	34.60	36.69	2.09
5H-2, 150	36.10	38.19	2.09
5H-3, 150	37.60	39.69	2.09
5H-4, 150	39.10	41.19	2.09
5H-5, 150	40.60	42.69	2.09
5H-6, 150	42.10	44.19	2.09
5H-7, 51	43.60	45.69	2.09
5H-CC, 24	44.11	46.20	2.09
6H-1, 150	44.10	45.71	1.61
6H-2, 150	45.60	47.21	1.61
6H-3, 150	47.10	48.71	1.61
6H-4, 150	48.60	50.21	1.61
6H-5, 150	50.10	51.71	1.61
6H-6, 150	51.60	53.21	1.61
6H-7, 63	53.10	54.71	1.61
6H-CC, 25	53.73	55.34	1.61
7H-1, 150	53.60	55.65	2.05
7H-2, 150	55.10	57.15	2.05
7H-3, 150	56.60	58.65	2.05
7H-4, 150	58.10	60.15	2.05
7H-5, 150	59.60	61.65	2.05
7H-6, 150	61.10	63.15	2.05
7H-7, 44	62.60	64.65	2.05
7H-CC, 26	63.04	65.09	2.05
8H-1, 150	63.10	71.22	8.12
8H-2, 150	64.60	72.72	8.12
8H-3, 150	66.10	74.22	8.12
8H-4, 150	67.60	75.72	8.12
8H-5, 150	69.10	77.22	8.12
8H-6, 150	70.60	78.72	8.12
8H-7, 59	72.10	80.22	8.12
8H-CC, 23	72.69	80.81	8.12
9H-1, 150	72.60	80.86	8.26
9H-2, 150	74.10	82.36	8.26
9H-3, 150	75.60	83.86	8.26
9H-4, 150	77.10	85.36	8.26
9H-5, 150	78.60	86.86	8.26
9H-6, 150	80.10	88.36	8.26
9H-7, 61	81.60	89.86	8.26
9H-CC, 27	82.21	90.47	8.26
10H-1, 150	82.10	91.15	9.05
10H-2, 150	83.60	92.65	9.05
10H-3, 150	85.10	94.15	9.05
10H-4, 150	86.60	95.65	9.05
10H-5, 150	88.10	97.15	9.05
10H-6, 150	89.60	98.65	9.05

APPENDIX A (continued).

Core, section, interval (cm)	Depth mbsf	Depth mcd	Depth mcd – mbsf
10H-7, 54	91.10	100.15	9.05
10H-CC, 23	91.64	100.69	9.05
11H-1, 150	91.60	101.18	9.58
11H-2, 150	93.10	102.68	9.58
11H-3, 150	94.60	104.18	9.58
11H-4, 150	96.10	105.68	9.58
11H-5, 150	97.60	107.18	9.58
11H-6, 150	99.10	108.68	9.58
11H-7, 64	100.60	110.18	9.58
11H-CC, 25	101.24	110.82	9.58
12H-1, 150	101.10	111.21	10.11
12H-2, 150	102.60	112.71	10.11
12H-3, 150	104.10	114.21	10.11
12H-4, 150	105.60	115.71	10.11
12H-5, 150	107.10	117.21	10.11
12H-6, 150	108.60	118.71	10.11
12H-7, 56	110.10	120.21	10.11
12H-CC, 24	110.66	120.77	10.11
13H-1, 150	110.60	121.30	10.70
13H-2, 150	112.10	122.80	10.70
13H-3, 150	113.60	124.30	10.70
13H-4, 150	115.10	125.80	10.70
13H-5, 150	116.60	127.30	10.70
13H-6, 150	118.10	128.80	10.70
13H-7, 65	119.60	130.30	10.70
13H-CC, 24	120.25	130.95	10.70
14H-1, 150	120.10	131.58	11.48
14H-2, 150	121.60	133.08	11.48
14H-3, 150	123.10	134.58	11.48
14H-4, 150	124.60	136.08	11.48
14H-5, 150	126.10	137.58	11.48
14H-6, 150	127.60	139.08	11.48
14H-7, 54	129.10	140.58	11.48
14H-CC, 22	129.64	141.12	11.48
15H-1, 150	129.60	142.18	12.58
15H-2, 150	131.10	143.68	12.58
15H-3, 150	132.60	145.18	12.58
15H-4, 150	134.10	146.68	12.58
15H-5, 150	135.60	148.18	12.58
15H-6, 150	137.10	149.68	12.58
15H-7, 57	138.60	151.18	12.58
15H-CC, 24	139.17	151.75	12.58
16H-1, 150	139.10	152.41	13.31
16H-2, 150	140.60	153.91	13.31
16H-3, 150	142.10	155.41	13.31
16H-4, 150	143.60	156.91	13.31
16H-5, 150	145.10	158.41	13.31
16H-6, 150	146.60	159.91	13.31
16H-7, 58	148.10	161.41	13.31
16H-CC, 21	148.68	161.99	13.31
17H-1, 150	148.60	163.15	14.55
17H-2, 150	150.10	164.65	14.55
17H-3, 150	151.60	166.15	14.55
17H-4, 150	153.10	167.65	14.55
17H-5, 150	154.60	169.15	14.55
17H-6, 150	156.10	170.65	14.55
17H-7, 60	157.60	172.15	14.55
17H-CC, 23	158.20	172.75	14.55
18H-1, 150	158.10	173.16	15.06
18H-2, 150	159.60	174.66	15.06
18H-3, 150	161.10	176.16	15.06
18H-4, 150	162.60	177.66	15.06
18H-5, 150	164.10	179.16	15.06
18H-6, 150	165.60	180.66	15.06
18H-7, 60	167.10	182.16	15.06
18H-CC, 21	167.70	182.76	15.06
19H-1, 150	167.60	184.38	16.78
19H-2, 150	169.10	185.88	16.78
19H-3, 150	170.60	187.38	16.78
19H-4, 150	172.10	188.88	16.78
19H-5, 150	173.60	190.38	16.78
19H-6, 150	175.10	191.88	16.78
19H-7, 63	176.60	193.38	16.78
19H-CC, 20	177.23	194.01	16.78
20H-1, 150	177.10	194.58	17.48
20H-2, 150	178.60	196.08	17.48
20H-3, 150	180.10	197.58	17.48
20H-4, 150	181.60	199.08	17.48
20H-5, 150	183.10	200.58	17.48
20H-6, 150	184.60	202.08	17.48
20H-7, 65	186.10	203.58	17.48
20H-CC, 26	186.75	204.23	17.48
21H-1, 150	186.60	205.35	18.75
21H-2, 150	188.10	206.85	18.75
21H-3, 150	189.60	208.35	18.75
21H-4, 150	191.10	209.85	18.75
21H-5, 150	192.60	211.35	18.75
21H-6, 150	194.10	212.85	18.75
21H-7, 60	195.60	214.35	18.75
21H-CC, 19	196.20	214.95	18.75
22H-1, 150	196.10	216.00	19.90
22H-2, 150	197.60	217.50	19.90
22H-3, 150	199.10	219.00	19.90
22H-4, 150	200.60	220.50	19.90
22H-5, 150	202.10	222.00	19.90
22H-6, 150	203.60	223.50	19.90
22H-7, 58	205.10	225.00	19.90
23H-1, 150	205.60	226.62	21.02
23H-2, 150	207.10	228.12	21.02
23H-3, 150	208.60	229.62	21.02
23H-4, 150	210.10	231.12	21.02
23H-5, 150	211.60	232.62	21.02
23H-6, 150	213.10	234.12	21.02
23H-CC, 30	214.60	235.62	21.02

APPENDIX B
Composite section (splice) tie points, Site 907.

Hole, core, section, interval (cm)	Depth (mbsf)	Depth (mcd)		Hole, core, section, interval (cm)	Depth (mbsf)	Depth (mcd)
A-1H-4, 120	5.70	5.70	tie to	B-2H-2, 117	5.37	5.70
B-2H-3, 117	6.87	7.20		C-2H-1, 24	6.34	7.20
C-2H-1, 134	7.44	8.30		A-2H-1, 97	8.27	8.30
A-2H-4, 140	13.20	13.23		C-2H-5, 27	12.37	13.23
C-2H-5, 146	13.56	14.42		B-3H-1, 65	12.85	14.42
B-3H-4, 32	17.02	18.59		C-3H-1, 80	16.40	18.59
C-3H-2, 68	17.78	19.97		A-3H-2, 17	18.47	19.97
A-3H-6, 140	25.70	27.20		C-4H-1, 17	25.27	27.20
C-4H-2, 87	27.47	29.42		A-4H-1, 39	26.69	29.42
A-4H-6, 146	35.26	37.99		C-5H-1, 130	35.90	37.99
C-5H-4, 139	40.49	42.58		A-5H-1, 83	36.63	42.58
A-5H-7, 22	45.02	50.97		C-6H-4, 76	49.36	50.97
C-6H-5, 16	50.26	51.87		A-6H-1, 78	46.08	51.87
A-6H-6, 149	54.29	60.08		C-7H-3, 143	58.03	60.08
C-7H-5, 55	60.15	62.20		A-7H-1, 67	55.47	62.20
A-7H-6, 112	63.42	70.15		B-8H-2, 22	61.42	70.15
B-8H-3, 111	63.81	72.54		A-8H-1, 50	64.80	72.54
A-8H-5, 34	70.64	78.38		C-8H-5, 116	70.26	78.38
C-8H-7, 16	72.26	80.38		B-9H-2, 52	71.22	80.38
B-9H-3, 15	72.35	81.51		C-9H-1, 65	73.25	81.51
C-9H-2, 5	74.15	82.41		A-9H-1, 95	74.75	82.41
A-9H-6, 87	82.27	89.83		B-10H-2, 34	80.53	89.83
B-10H-3, 88	82.58	91.88		A-10H-1, 44	83.74	91.88
A-10H-6, 14	90.94	99.08		B-11H-1, 97	89.17	99.08
B-11H-3, 102	92.22	102.13		A-11H-1, 92	93.72	102.13
A-11H-7, 7	101.88	110.29		B-12H-2, 125	100.45	110.29
B-12H-5, 82	104.52	114.36		A-12H-2, 149	105.29	114.36
A-12H-6, 135	111.15	120.24		B-13H-2, 103	109.73	120.24
B-13H-4, 110	112.80	123.30		A-13H-1, 59	112.39	123.30
A-13H-6, 148	120.78	131.69		C-14H-1, 11	120.21	131.69
C-14H-2, 31	121.91	133.39		A-14H-2, 8	122.89	133.39
A-14H-6, 119	129.99	140.49		B-15H-2, 81	128.51	140.49
B-15H-4, 98	131.68	143.67		A-15H-1, 107	131.87	143.67
A-15H-6, 28	138.69	150.39		B-16H-2, 44	137.64	150.39
B-16H-5, 57	141.19	153.94		A-16H-1, 138	141.68	153.94
A-16H-6, 78	148.58	160.84		B-17H-2, 62	147.32	160.84
B-17H-4, 48	150.17	163.69		A-17H-1, 94	150.74	163.69
A-17H-6, 145	158.75	171.69		B-18H-2, 29	156.49	171.69
B-18H-3, 136	159.06	174.26		C-18H-1, 110	159.20	174.26
C-18H-3, 121	162.31	177.37		A-18H-3, 38	162.68	177.37
A-18H-6, 61	167.41	182.09		B-19H-1, 142	165.62	182.09
B-19H-4, 19	168.89	185.36		C-19H-1, 98	168.58	185.36
C-19H-2, 103	170.13	186.91		A-19H-1, 68	169.48	186.91
A-19H-7, 28	178.11	195.54		C-20H-1, 96	178.06	195.54
C-20H-3, 61	180.71	204.94		A-20H-2, 43	180.23	198.19
A-20H-6, 118	186.98	198.19		B-21H-3, 33	186.53	204.94
B-21H-3, 122	187.41	205.82		C-21H-1, 47	187.07	205.82
C-21H-3, 54	190.14	208.89		A-21H-2, 17	189.47	208.89
A-21H-6, 147	196.77	216.19		B-22H-3, 42	196.12	216.19
B-22H-5, 8	198.78	218.84		A-22H-2, 51	199.31	218.84
A-22H-6, 75	205.15	224.68		B-23H-2, 63	204.33	224.68
B-23H-4, 146	208.16	228.95		A-23H-2, 125	209.55	228.95